PHYSICAL REVIEW D **89,** 125005 (2014)

Contribution of plasminos to the shear viscosity of a hot and dense Yukawa-Fermi gas

N. Sadooghi* and F. Taghinavaz†

Department of Physics, Sharif University of Technology, P.O. Box 11155-9161, Tehran, Iran

(Received 10 April 2014; published 5 June 2014)

We determine the shear viscosity of a hot and dense Yukawa-Fermi gas, using the standard Green-Kubo relation, according to which the shear viscosity is given by the retarded correlator of the traceless part of the viscous energy-momentum tensor. We approximate this retarded correlator using a one-loop skeleton expansion, and express the bosonic and fermionic shear viscosities, η_b and η_f, in terms of bosonic and fermionic spectral widths, Γ_b and $\Gamma_\pm$. Here, the subscripts $\pm$ correspond to normal and collective (plasmino) excitations of fermions. We study, in particular, the effect of these excitations on thermal properties of $\eta_f[\Gamma_\pm]$. To do this, we determine first the dependence of Γ_b and $\Gamma_\pm$ on momentum p, temperature T, chemical potential μ and $\xi_0 \equiv m_b^0/m_f^0$, in a one-loop perturbative expansion in the orders of the Yukawa coupling. Here, m_b^0 and m_f^0 are T- and μ-independent bosonic and fermionic masses, respectively. We then numerically determine $\eta_b[\Gamma_b]$ and $\eta_f[\Gamma_\pm]$, and study their thermal properties. It turns out that whereas Γ_b and Γ_+ decrease with increasing T or μ, Γ_- increases with increasing T or μ. This behavior qualitatively changes by adding thermal corrections to m_b^0 and m_f^0, while the difference between Γ_+ and Γ_- keeps increasing with increasing T or μ. Moreover, η_b (η_f) increases (decreases) with increasing T or μ. We show that the effect of plasminos on η_f becomes negligible with increasing (decreasing) T (μ).

DOI: 10.1103/PhysRevD.89.125005 PACS numbers: 11.10.Wx, 12.38.Mh, 51.20.+d, 52.25.Fi

I. INTRODUCTION

One of the main goals of the modern experiments of ultra-relativistic heavy-ion collisions is to clarify the nature of the phase transition of QCD. As predicted from numerical computations on the lattice, at a temperature of about 150 MeV, quark matter undergoes a phase transition, during which hadrons melt and a new state of matter—a plasma of quarks and gluons—is built. There is strong evidence for the creation of the quark-gluon plasma (QGP) in heavy-ion experiments at the Relativistic Heavy-Ion Collider (RHIC) and the Large Hadron Collider (LHC) [1]. The experimental results show that the elliptic flow, v_2, describing the azimuthal asymmetry in momentum space, is the largest ever seen in heavy-ion collisions [2]. The elliptic flow v_2 is proportional to the initial eccentricity $\epsilon_2 \equiv |\langle r^2 e^{2i\phi}\rangle|/\langle r^2\rangle$ of a given collision, which describes the asymmetric region of overlap in a collision between two nuclei and results in an anisotropy in the transverse density of the system at the early stages of the collision [3]. The collective response of the system—well-described by viscous hydrodynamics—transforms this spatial anisotropy into a momentum anisotropy. Thus, v_2 is proportional to ϵ_2, with the proportionality factor depending on the shear viscosity η of the medium [3]. The latter characterizes the diffusion of momentum transverse to the direction of propagation. The comparison between the experimentally measured v_2 and the results arising from second-order viscous hydrodynamics has suggested that the new state of matter created at RHIC and LHC is an almost perfect fluid, having a very small shear viscosity to entropy density ratio η/s [4,5] (see also Ref. [6] for a recent review on the status of η/s). However, as was reported in Ref. [6], in all hydrodynamic simulations performed so far, the shear viscosity is assumed to be temperature independent.

The shear viscosity is one of the transport coefficients, which describe the properties of a system out of equilibrium, and can theoretically be determined using two different approaches: the kinetic theory approach, based on the Boltzmann equation for the corresponding momentum distribution function [7–9], and the Green-Kubo approach in the framework of linear response theory [10], in which all transport coefficients are formulated in terms of retarded correlators of the energy-momentum tensor [11,12]. The advantage of the second method is that it provides a framework where the transport coefficients can be computed using equilibrium thermal field theory. Other alternative methods to compute transport coefficients are direct numerical simulations on a space-time lattice [13], using a two-particle-irreducible effective action [14], and holographic models [15]. A novel diagrammatic method was also presented in Ref. [16]. The aim of most of these computations is to determine the dependence of η on temperature and chemical potential [17–19] or on external electromagnetic fields [20].

In this paper, we use the Green-Kubo formalism to determine the dependence of the shear viscosity of a Yukawa-Fermi gas on temperature, chemical potential,

*sadooghi@physics.sharif.ir
†taghinavaz@physics.sharif.ir

and bosonic and fermionic masses. Thermal corrections to the masses of bosons and fermions will be considered too and their effect on the shear viscosity will be scrutinized. Our approach is similar to what was recently presented by Lang *et al.* in Refs. [18,19]. In Ref. [18], an appropriate skeleton expansion was used to approximate the retarded correlators appearing in the Kubo relation for the shear viscosities of a real $\lambda\varphi^4$ theory and an interacting pion gas. Using the standard Källen-Lehmann representation of a retarded two-point Green's function in terms of the interacting bosonic spectral function, ρ_b, the shear viscosity of the scalar and pseudoscalar bosons, η_b, is then expressed in terms of the real and imaginary parts of the retarded two-point Green's function. The latter, denoted by Γ_b, defines, in particular, the spectral width of the bosons and is inversely proportional to their mean free path. To approximate the bosonic correlators, a systematic Laurent expansion of η_b in orders of Γ_b is performed. The series is then truncated at the leading Γ_b^{-1} order. Then, by computing Γ_b perturbatively in orders of the small coupling constant of the theory up to the first non-vanishing contribution, the T dependence of the bosonic shear viscosity is numerically determined. In Ref. [19], almost the same method was used to determine the fermionic shear viscosity, η_f, of a strongly interacting quark matter, described by a two-flavor Nambu–Jona-Lasinio (NJL) model [21], which consists of a four-fermion interaction with no gluons involved. To do this, η_f is first expressed in terms of the fermionic spectral function, ρ_f, and then—working, as in Ref. [22], in a quasiparticle approximation—a generalized Breit-Wigner shape for the fermionic spectral function is used to formulate η_f in terms of the quasiparticle mass M and width Γ_f. Using then four different parametrizations for Γ_f, the thermal properties of η_f is explored. Eventually, the constant quasiparticle mass M is replaced with the T- and μ-dependent, dynamically generated constituent quark mass of the NJL model, and the thermal properties of η_f are qualitatively studied in the vicinity of the chiral transition point.

In the present paper, we will compute the shear viscosity of an interacting boson-fermion system with the Yukawa coupling. In this theory, the shear viscosity consists of a bosonic part and a fermionic part. Following the method presented in Ref. [18], we will first derive η_b in terms of Γ_b in a systematic Laurent expansion up to $\mathcal{O}(\Gamma_b^0)$. Performing then a one-loop perturbative expansion in orders of the Yuwaka coupling, we will determine Γ_b as a function of momentum p, temperature T, chemical potential μ and $\xi_0 \equiv m_b^0/m_f^0$, where m_b^0 and m_f^0 are constant bosonic and fermionic masses. Using $\eta_b[\Gamma_b]$, we will study the T and μ dependence of the bosonic shear viscosity for various ξ_0. We will then add the thermal masses of bosons and fermions to m_b^0 and m_f^0, and study the effect of thermal masses on Γ_b and η_b. Thermal corrections to the masses of bosons and fermions are computed using the standard hard-thermal-loop (HTL) method (see e.g. Ref. [23]). Let us notice that, according to the description in Ref. [24], this *ad hoc* treatment of thermal masses seems intuitive and is justified, since it equals the HTL treatment with an approximate fermion propagator. However, it is not equal to the full HTL result [23].

We will then focus on the fermionic part of the shear viscosity, and derive its dependence on the fermionic spectral width. This builds the central part of the analytical results of the present paper. Here, in contrast to the approximations made in Ref. [19], we use the spectral representation of the retarded two-point Green's function presented for the first time in Ref. [25] (see also Ref. [26]). The latter was used in Refs. [23,27–35] within the context of Yukawa theory, the NJL model, QED and QCD. In Ref. [25], it was shown that a fermionic system at finite temperature has twice as many fermionic modes as one at zero temperature. Besides propagating quarks and antiquarks, there are also propagating quark holes and antiholes. Thus, thermal fermions have, apart from normal excitation, a collective excitation, referred to as either a hole or a plasmino [26]. The latter appears as an additional pole in the fermion propagator, and as a consequence of the preferred frame defined by the heat bath. Hence, the two poles lead to two different dispersion relations, both with positive energy. It turns out that in the chiral limit $m_f^0 \to 0$, the normal excitation has the same chirality and helicity, while the collective excitation possesses opposite chirality and helicity [26]. Denoting the spectral widths, corresponding to the normal and collective (plasmino) excitations, with Γ_+ and Γ_-, respectively, we will use the aforementioned Laurent expansion to derive a novel analytic relation for η_f in terms of $\Gamma_\pm$ up to $\mathcal{O}(\Gamma_\pm^0)$. We will then determine the p, T, μ and ξ_0 dependence of $\Gamma_\pm$ in a one-loop perturbative expansion in orders of the Yukawa coupling. Using $\eta_f[\Gamma_\pm]$, it is then possible to explore the thermal properties of η_f for various ξ_0. Adding thermal corrections to the bosonic and fermionic masses, the effect of thermal masses on $\Gamma_\pm$ and η_f will also be studied. Let us notice at this stage that in the literature [17,29,33], the difference between Γ_+ and Γ_-, as well as their p dependence are often neglected, and $\Gamma_\pm(p)$ is approximated by $\Gamma_\pm(0) \propto g^2 T$, where g is the coupling constant of the theory [17,33]. We, however, will explicitly determine the p dependence of Γ_+ and Γ_-, and use it in the numerical computation of η_f. Then, we will assume $\Gamma_+ = \Gamma_-$, and we will determine the difference between $\eta_f[\Gamma_+ \neq \Gamma_-]$ and $\eta_f[\Gamma_+ = \Gamma_-]$ in terms of T and μ. It turns out that, depending on T and/or μ, $\eta_f[\Gamma_+ = \Gamma_-]$ is larger than $\eta_f[\Gamma_+ \neq \Gamma_-]$.

The organization of this paper is a follows. In Sec. II, we will review the Green-Kubo formalism, and present the shear viscosity in terms of retarded correlators of the traceless part of the viscous energy-momentum tensor. In Sec. III, we start with the Lagrangian density of the Yukawa theory, and derive the bosonic and fermionic contributions to the shear viscosity, in a one-loop skeleton expansion, in terms of bosonic and fermionic spectral density functions, ρ_b and ρ_f. Eventually, using an appropriate Laurent expansion in orders of bosonic and fermionic spectral widths, $\eta_b[\Gamma_b]$ and $\eta_f[\Gamma_\pm]$ are determined (see Secs. III A and III B as well as Appendices A and C). In Sec. IV, the spectral bosonic and fermionic widths, Γ_b and $\Gamma_\pm$ are separately computed in a one-loop perturbative expansion in orders of the Yukawa coupling (see Sec. IV A for the bosonic and Sec. IV B for the fermionic spectral widths). In order to derive the imaginary part of the retarded two-point Green's functions, corresponding to bosons and fermions, the standard Schwinger-Keldysh real-time formalism [36] is used. We will mainly use the notations of Refs. [37] and [38]. In Sec. V, we will present our numerical results. Here, the T, μ and ξ_0 dependence of Γ_b and $\Gamma_\pm$, as well as the thermal properties of $\eta_b[\Gamma_b]$ and $\eta_f[\Gamma_\pm]$, will be explored. As it turns out, Γ_b and Γ_+ decreases with increasing T or μ. In contrast, Γ_- increases with increasing T or μ. Whereas this behavior changes when thermal corrections are added to m_b^0 and m_f^0, Γ_+ and Γ_- still exhibit different T and μ dependencies. This difference increases with increasing T or μ. As concerns the shear viscosities, η_b (η_f) increases (decreases) with increasing T or μ. Moreover, it turns out that the contribution of plasminos to η_f becomes negligible with increasing (decreasing) T (μ). A summary of our results is presented in Sec. VI.

II. SHEAR VISCOSITY IN RELATIVISTIC HYDRODYNAMICS

An ideal and locally equilibrated relativistic fluid is mainly described by the dynamics of the corresponding energy-momentum tensor

$$T_0^{\mu\nu} = \epsilon u^\mu u^\nu + P\Delta^{\mu\nu}, \tag{2.1}$$

where ϵ is the energy density, P is the pressure and $u_\mu(x) = \gamma(x)(1, \mathbf{v}(x))$ is the four-velocity of the fluid, which is defined by the variation of the four-coordinate x^μ with respect to the proper time τ. Here, the Lorentz factor $\gamma(x) \equiv (1 - \mathbf{v}^2(x))^{-1}$. In Eq. (2.1), $\Delta^{\mu\nu}$ is defined by $\Delta^{\mu\nu} \equiv g^{\mu\nu} - u^\mu u^\nu$, with the metric $g^{\mu\nu} = \mathrm{diag}(+,-,-,-)$. It satisfies $u_\mu \Delta^{\mu\nu} = 0$. Moreover, for the four-velocity u_μ, we have $u_\mu u^\mu = 1$. If there are no external sources, the energy-momentum tensor (2.1) is conserved,

$$\partial_\mu T_0^{\mu\nu} = 0. \tag{2.2}$$

Apart from Eq. (2.2), an ideal fluid is characterized by the entropy current conservation law $\partial_\mu s^\mu = 0$, where the entropy current, $s_\mu \equiv s u_\mu$, includes the entropy density s. In a system without conserved charges, ϵ and P satisfy $\epsilon + P = Ts$, where T is the local temperature of the fluid.

To include dissipative effects to the fluid, the viscous stress tensor $\tau^{\mu\nu}$ is to be added to $T_0^{\mu\nu}$ from Eq. (2.1). The total energy-momentum tensor then reads

$$T^{\mu\nu} = T_0^{\mu\nu} + \tau^{\mu\nu}, \tag{2.3}$$

where $\tau^{\mu\nu}$ satisfies $u_\mu \tau^{\mu\nu} = 0$. In an expansion in orders of derivatives of u_μ, the viscous stress tensor is determined using the second law of thermodynamics, $T\partial_\mu s^\mu \geq 0$, which replaces the conservation law $\partial_\mu s^\mu = 0$ of the ideal fluid. The viscous stress tensor is often split as

$$\tau^{\mu\nu} = \pi^{\mu\nu} + \Delta^{\mu\nu}\Pi, \tag{2.4}$$

where $\pi^{\mu\nu}$ is the traceless part ($\pi^\mu{}_\mu = 0$) and Π is the remaining part with nonvanishing trace. Each part of $\tau^{\mu\nu}$ is then parametrized by a number of viscous coefficients. In the first-order derivative expansion, $\tau^{\mu\nu}$ is characterized by the shear and bulk viscosities, η and ζ, that appear in the traceless part of $\tau^{\mu\nu}$,

$$\pi^{\mu\nu} = \eta\left(\nabla^\mu u^\nu + \nabla^\nu u^\mu - \frac{2}{3}\Delta^{\mu\nu}\nabla^\rho u_\rho\right), \tag{2.5}$$

and in the part of $\tau^{\mu\nu}$ with nonvanishing trace,

$$\Pi = \zeta \nabla^\mu u_\mu, \tag{2.6}$$

respectively. Here, $\nabla^\mu \equiv \Delta^{\mu\nu}\partial_\nu$. Using the properties of $\Delta^{\mu\nu}$ in $d = 4$-dimensional space-time, $\Delta^{\mu\nu}u_\nu = 0$ as well as $\Delta_\mu^\rho \Delta_\nu^\mu = \Delta^\rho{}_\nu$, we get

$$\epsilon = u_\mu u_\nu T^{\mu\nu}, \qquad P = -\frac{1}{3}\Delta_{\mu\nu}T^{\mu\nu}, \tag{2.7}$$

as well as

$$\tilde{\pi}^{\mu\nu} = \left(\Delta^{\rho\mu}\Delta^{\sigma\nu} + \Delta^{\rho\nu}\Delta^{\sigma\mu} - \frac{2}{3}\Delta^{\mu\nu}\Delta^{\rho\sigma}\right)T_{\rho\sigma}. \tag{2.8}$$

Here, $\tilde{\pi}^{\mu\nu} \equiv \eta^{-1}\pi^{\mu\nu}$ is introduced. In the rest of this paper, we will focus on the shear viscosity η. Following Zubarev's approach [10] and within linear response theory, it is determined by the Kubo-type formula [18],

$$\eta = \frac{\beta_s}{10}\int d^3x' \int_{-\infty}^{t} dt' (\tilde{\pi}^{\mu\nu}(0), \tilde{\pi}_{\mu\nu}(\mathbf{x}', t')), \tag{2.9}$$

where the inverse proper temperature $\beta_s \equiv \gamma\beta$ with $\beta \equiv T^{-1}$, and

$$(X, Y) = \frac{1}{\beta}\int_0^\beta d\tau \langle X[e^{H\tau} Y e^{-H\tau} - \langle Y\rangle_0]\rangle_0. \tag{2.10}$$

Here, H is the free part of the Hamiltonian of a fully interacting theory, which is given in terms of the energy-momentum tensor $T^{\mu\nu}$, via $\beta H = \int d^3x \beta_s(\mathbf{x}, \tau) u^\mu(\mathbf{x}, \tau) T_{0\mu}(\mathbf{x}, \tau)$. Moreover, $\langle \cdots \rangle_0$ is the thermal expectation value with respect to the equilibrium statistical operator ρ_0, and is defined by $\langle \cdot \rangle_0 = \mathrm{tr}(\cdot \rho_0)$ [18].

The correlator appearing in Eq. (2.9) can be expressed as a real-time integral over a retarded correlator,

$$(X(t), Y(t')) \sim -\frac{1}{\beta}\int_{-\infty}^{t'} dt'' \langle X(t), Y(t'')\rangle_R, \tag{2.11}$$

with

$$\langle X(t), Y(t')\rangle_R = -i\theta(t-t')\langle [X(t), Y(t')]\rangle_0. \tag{2.12}$$

In the large-time limit $t' \to \infty$, when the system approaches global equilibrium, the approximation appearing in Eq. (2.11) becomes exact. Combining at this stage Eqs. (2.9) and (2.11), and evaluating the resulting expression in the local rest frame, where $\beta_s = \beta$, the Kubo-formula for the shear viscosity reads

$$\eta = -\frac{1}{10}\int_{-\infty}^{0} dt \int_{-\infty}^{t} dt' \Pi_R(t'), \tag{2.13}$$

with the retarded Green's function

$$\Pi_R(t) \equiv -i\theta(-t)\int d^3x \langle [\tilde{\pi}^{\mu\nu}(0), \tilde{\pi}_{\mu\nu}(\mathbf{x}, t)]\rangle_0, \tag{2.14}$$

and $\tilde{\pi}^{\mu\nu}$ given in Eq. (2.8). Equivalently η is given by

$$\eta = \frac{i}{10}\frac{d}{dp_0}\Pi_R(p_0)|_{p_0=0}. \tag{2.15}$$

It arises by replacing the Fourier transformation of $\Pi_R(t) = \int \frac{dp_0}{2\pi} e^{-ip_0 t}\Pi_R(p_0)$ in Eq. (2.13), and integrating over t and t' using the functional identity [18]

$$\int_{-\infty}^{0} dt' \int_{t}^{0} dt e^{-ip_0 t'} \to -2\pi i\delta(p_0)\frac{d}{dp_0}. \tag{2.16}$$

It is the purpose of this paper to determine the thermal properties of the shear viscosity of a Yukawa theory by computing Π_R from Eq. (2.14) in a weak coupling expansion in orders of the Yukawa coupling. To this purpose, we will first introduce a Yukawa theory including a real scalar and a fermionic field, and then, using an appropriate weak coupling expansion up to the one-loop level, we will determine η for these fields separately.

III. SHEAR VISCOSITY OF A YUKAWA THEORY: GENERAL CONSIDERATIONS

In this section, we will first review the method presented in Ref. [18], and determine the bosonic part of the shear viscosity of a Yukawa theory in terms of the bosonic spectral width. We will then use this method as a guideline, and derive the fermionic part of the shear viscosity of the Yukawa theory in terms of fermionic spectral widths. Here, we will explicitly consider the contributions of the normal and collective (plasmino) excitations of fermions, with different spectral widths. This is in contrast with the result recently presented in Ref. [19], where within a quasiparticle approximation, a Breit-Wigner type formula was presented for the fermionic shear viscosity in terms of one and the same fermionic spectral width.

Let us start with the Lagrangian density of a Yukawa theory,

$$\mathcal{L} = \bar{\psi}(i\gamma\cdot\partial - m_f)\psi + \frac{1}{2}\partial_\mu\varphi\partial^\mu\varphi - \frac{1}{2}m_b^2\varphi^2 + g\bar{\psi}\psi\varphi, \tag{3.1}$$

where, φ is a real scalar field and $\bar{\psi}, \psi$ are fermionic fields. Moreover, m_b and m_f correspond to the masses of bosons and fermions, respectively. According to Eq. (2.13), the shear viscosity η for this theory is given by a two-point Green's function of the tensor field $\tilde{\pi}^{\mu\nu}$, which is defined in Eq. (2.8) in terms of the energy-momentum tensor $T_{\mu\nu}$. The energy-momentum tensor of the Yukawa theory is given by

$$T_{\mu\nu} = i\bar{\psi}\gamma_\mu\partial_\nu\psi + \partial_\mu\varphi\partial_\nu\varphi - \mathcal{L}g_{\mu\nu}, \tag{3.2}$$

where $\mathcal{L}$ is given in Eq. (3.1). As it turns out, $T_{\mu\nu}$, and consequently the shear viscosity include a bosonic part and a fermionic part. In what follows, we will denote them by η_b and η_f, where the subscripts correspond to bosons (b) and fermions (f). To compute these two parts separately, we will use Eq. (2.15). Introducing the imaginary time $\tau \equiv it$ in Eq. (2.14), the thermal Green's function, $\Pi_T(\tau)$, reads

$$\Pi_T(\tau) \equiv \int d^3x \langle \mathcal{T}_\tau[\tilde{\pi}^{\mu\nu}(0)\tilde{\pi}_{\mu\nu}(\mathbf{x}, \tau)]\rangle_0, \tag{3.3}$$

where $\mathcal{T}_\tau$ stands for the time-ordering prescription. According to the above descriptions, it is given by

$$\Pi_T(\tau) = \Pi_T^b(\tau) + \Pi_T^f(\tau), \tag{3.4}$$

with the bosonic part

$$\Pi_T^b(\tau) = 2\int d^3x\eta^{\alpha\beta\rho\sigma} \times \langle \partial_\beta\varphi(0)\partial_\rho\varphi(0)\partial_\alpha\varphi(\mathbf{x}, \tau)\partial_\sigma\varphi(\mathbf{x}, \tau)\rangle_0, \tag{3.5}$$

and the fermionic part

$$\Pi_T^f(\tau) = -2\int d^3x\eta^{\alpha\beta\rho\sigma} \times \langle \bar{\psi}(0)\gamma_\beta\partial_\rho\psi(0)\bar{\psi}(\mathbf{x}, \tau)\gamma_\alpha\partial_\sigma\psi(\mathbf{x}, \tau)\rangle_0. \tag{3.6}$$

In the above relations, $\eta^{\alpha\beta\rho\sigma}$ is defined by

$$\eta^{\alpha\beta\rho\sigma} \equiv \Delta^{\alpha\beta}\Delta^{\rho\sigma} + \Delta^{\beta\sigma}\Delta^{\rho\alpha} - \frac{2}{3}\Delta^{\alpha\sigma}\Delta^{\beta\rho}. \quad (3.7)$$

By performing a Fourier transformation into the momentum space, using $\tilde{\varphi}(\mathbf{p},\tau) = \int d^3x e^{i\mathbf{p}\cdot\mathbf{x}}\varphi(\mathbf{x},\tau)$ and $\tilde{\psi}(\mathbf{p},\tau) = \int d^3x e^{i\mathbf{p}\cdot\mathbf{x}}\psi(\mathbf{x},\tau)$, evaluating the resulting four-point functions arising in Eqs. (3.5) and (3.6) using an appropriate expansion up to the one-loop skeleton expansion, as was described in Ref. [18], and eventually neglecting the disconnected parts of the Green's functions, the bosonic part of $\Pi_T(\tau)$ reads

$$\Pi_T^b(\omega_n) = 4\int_0^\beta d\tau e^{i\omega_n\tau} \times \int \frac{d^3p}{(2\pi)^3}\eta^{\alpha\beta\rho\sigma}p_\alpha p_\beta p_\rho p_\sigma G_T^2(\mathbf{p},\tau), \quad (3.8)$$

and the fermionic part of $\Pi_T(\tau)$ is given by

$$\Pi_T^f(\omega_n) = 2\int_0^\beta d\tau e^{i\omega_n\tau}\int \frac{d^3p}{(2\pi)^3}\eta^{\alpha\beta\rho\sigma}p_\rho p_\sigma \times \mathrm{tr}[S_T(\mathbf{p},\tau)\gamma_\alpha S_T(\mathbf{p},-\tau)\gamma_\beta]. \quad (3.9)$$

Let us notice that in the above relations $G_T(\mathbf{p},\tau)$ and $S_T(\mathbf{p},\tau)$ are exact (dressed) bosonic and fermionic two-point functions, respectively. They are defined by

$$G_T(\mathbf{p},\tau) \equiv V^{-1}\langle T_\tau[\tilde{\varphi}(0)\tilde{\varphi}(\mathbf{p},\tau)]\rangle_0, \quad (3.10)$$

and

$$S_T(\mathbf{p},\tau) \equiv V^{-1}\langle T_\tau[\tilde{\psi}(0)\tilde{\bar{\psi}}(\mathbf{p},\tau)]\rangle_0. \quad (3.11)$$

Moreover, in Eqs. (3.8) and (3.9), the bosonic and fermionic Matsubara frequencies are given by $\omega_n = 2n\pi T$ and $\omega_n = (2n+1)\pi T$, respectively. As aforementioned, the expressions presented in Eqs. (3.8) and (3.9) are the one-loop contributions in the skeleton expansion. The latter is diagrammatically presented in Fig. 1. In what follows, we will separately evaluate the bosonic and fermionic thermal two-point functions (3.8) and (3.9). The results will then be used to determine the bosonic and fermionic parts of the shear viscosity η in term of bosonic and fermionic spectral widths.

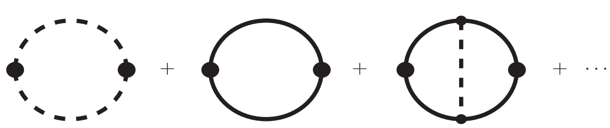

FIG. 1. The skeleton expansion of $\Pi_T(\tau)$ from Eq. (3.3). Dashed and solid lines denote the dressed bosonic and fermionic two-point functions $G_T(\mathbf{p},\tau)$ from Eq. (3.10) and $S_T(\mathbf{p},\tau)$ from Eq. (3.11), respectively. In our computation up to the one-loop skeleton expansion, only the first two diagrams in the above series are considered.

A. The bosonic contribution to η in the one-loop skeleton expansion

To evaluate the bosonic part of the shear viscosity η_b, we will use the method described in Ref. [18], whose main steps will be reviewed in what follows.

Let us first consider Eq. (3.8). According to the standard Källen-Lehmann representation, the two-point Green's function $G_T(\mathbf{p},\omega_n)$ is given in terms of the bosonic spectral density function $\rho_b(\mathbf{p},\omega)$ as

$$G_T(\mathbf{p},\omega_n) = \frac{1}{2\pi}\int_{-\infty}^{+\infty} d\omega \frac{\rho_b(\mathbf{p},\omega)}{\omega + i\omega_n}. \quad (3.12)$$

Plugging this relation into

$$G_T(\mathbf{p},\tau) = \sum_{n=-\infty}^{+\infty} e^{-i\omega_n\tau}G_T(\mathbf{p},\omega_n), \quad (3.13)$$

and adding over bosonic Matsubara frequencies $\omega_n = 2n\pi T$, we arrive at

$$G_T(\mathbf{p},\tau) = \frac{1}{2\pi}\int_{-\infty}^{+\infty} d\omega e^{-\omega|\tau|}\rho_b(\mathbf{p},\omega)[1+n_b(\omega)], \quad (3.14)$$

where, the bosonic distribution function $n_b(\omega)$ reads

$$n_b(\omega) \equiv \frac{1}{e^{\beta\omega}-1}. \quad (3.15)$$

To derive Eq. (3.14), we have used the symmetry property $\rho_b(\mathbf{p},-\omega) = -\rho_b(\mathbf{p},\omega)$, which yields, in particular, $|\tau|$ on the rhs of Eq. (3.14). Further, by plugging $G_T(\mathbf{p},\tau)$ from Eq. (3.14) into Eq. (3.8), and integrating over τ, we arrive after analytical continuation, $i\omega_n \to p_0 + i\epsilon$, at

$$\Pi_R^b(p_0) = 4\int \frac{d^3p}{(2\pi)^3}\eta^{\alpha\beta\rho\sigma}p_\alpha p_\beta p_\rho p_\sigma \times \int_{-\infty}^{+\infty}\frac{d\omega_1 d\omega_2}{(2\pi)^2}\rho_b(\mathbf{p},\omega_1)\rho_b(\mathbf{p},\omega_2) \times n_b(\omega_1)n_b(\omega_2)W_\epsilon(\omega_{12},p_0), \quad (3.16)$$

where $\eta^{\alpha\beta\rho\sigma}$ is defined in Eq. (3.7), $\omega_{12} \equiv \omega_1 + \omega_2$, and $W_\epsilon(\omega_{12},p_0)$ is given by

$$W_\epsilon(\omega_{12},p_0) \equiv \frac{1}{p_0 + i\epsilon - \omega_{12}} - \frac{1}{p_0 + i\epsilon + \omega_{12}}. \quad (3.17)$$

At this stage, we use the definition of the bosonic spectral density function ρ_b in terms of the retarded two-point Green's function, $G_R(p)$,

$$\rho_b(p) \equiv -2\mathfrak{Im}[G_R(p)], \tag{3.18}$$

to formulate ρ_b in terms of the bosonic renormalized energy

$$E_b(p) \equiv \sqrt{\omega_b^2 + \mathfrak{Re}[\Sigma_R^b(p)]}, \tag{3.19}$$

with $\omega_b^2 \equiv \mathbf{p}^2 + m_b^2$, and the bosonic spectral width

$$\Gamma_b(p) \equiv -\frac{1}{2p_0}\mathfrak{Im}[\Sigma_R^b(p)]. \tag{3.20}$$

Using

$$\begin{aligned} G_R^{-1}(p) &= p^2 - m_b^2 - \Sigma_R^b(p) \\ &\simeq [p_0 + i\Gamma_b(p)]^2 - E_b^2(p), \end{aligned} \tag{3.21}$$

the bosonic spectral density function (3.18) is given by

$$\rho_b(\mathbf{p},\omega) = \frac{4\omega\Gamma_b(\mathbf{p},\omega_b)}{[\omega^2 - E_b^2(\mathbf{p},\omega_b) - \Gamma_b^2(\mathbf{p},\omega_b)]^2 + 4\omega^2\Gamma_b^2(\mathbf{p},\omega_b)}, \tag{3.22}$$

where $E_b = E_b(\mathbf{p},\omega_b)$ and $\Gamma_b = \Gamma_b(\mathbf{p},\omega_b)$ are to be evaluated on mass shell. Now, by plugging $\rho_b(\mathbf{p},\omega)$ from Eq. (3.22) into Eq. (3.16), and using [18]

$$\frac{i}{10}\frac{d}{dp_0}W_\epsilon(\omega_{12},p_0) = -\frac{\pi}{5}\delta'(\omega_{12}), \tag{3.23}$$

we arrive first at

$$\eta_b = \frac{4\beta}{5\pi}\int\frac{d^3p}{(2\pi)^3}\eta^{\alpha\beta\rho\sigma}p_\alpha p_\beta p_\rho p_\sigma\int_{-\infty}^{+\infty}d\omega F_b(\mathbf{p},\omega), \tag{3.24}$$

with $\omega \equiv \frac{1}{2}\bar{\omega}_{12} \equiv \frac{1}{2}(\omega_1 - \omega_2)$ and where $F_b(\mathbf{p},\omega)$ is given by

$$F_b(\mathbf{p},\omega) = \frac{2\omega^2 e^{\beta\omega}}{(e^{\beta\omega}-1)^2}\frac{\Gamma_b^2}{[E_b^2 - (\omega - i\Gamma_b)^2]^2[E_b^2 - (\omega + i\Gamma_b)^2]^2}. \tag{3.25}$$

Further, by plugging Eq. (3.25) into Eq. (3.24) and integrating over ω, using the same procedure as in Ref. [18] (which will be described below), we arrive at the bosonic part of the shear viscosity of the Yukawa theory in terms of the renormalized energy E_b from Eq. (3.19) and the bosonic spectral width Γ_b from Eq. (3.20),

$$\eta_b = \frac{\beta}{30\pi^2}\int_0^\infty dp\frac{\mathbf{p}^6}{E_b^2}\frac{e^{\beta E_b}}{(e^{\beta E_b}-1)^2}\frac{1}{\Gamma_b} + \mathcal{O}(\Gamma_b^0). \tag{3.26}$$

To derive Eq. (3.26), the pole structure of $F_b(\mathbf{p},\omega)$ from Eq. (3.25) is to be considered. Following Ref. [18], the integral over ω in Eq. (3.24) is to be performed by closing the contour in the upper half-plane, i.e. by considering only two poles $\omega^\pm \equiv \pm E_b + i\Gamma_b$ from four poles $\omega^\pm$ and $-\omega^\pm$, and eventually expanding the resulting analytical expression in orders of small Γ_b. This results in

$$2\pi i\sum_{\omega=\omega_b^\pm}F_b(\omega) = \frac{e^{\beta E_b}}{(e^{\beta E_b}-1)^2}\frac{\pi}{16E_b^2\Gamma_b} + \mathcal{O}(\Gamma_b^0). \tag{3.27}$$

Let us notice that apart from the aforementioned poles $\omega^\pm$ and $-\omega^\pm$, there are also an infinite number of poles arising from the denominator $e^{\beta\omega} - 1$ in Eq. (3.25). But as it was shown in Ref. [18], the contributions of their residues are proportional to Γ_b^2, and, if we assume that Γ_b is small enough, they are suppressed relative to the leading Γ_b^{-1} term in Eq. (3.27). Therefore, by plugging Eq. (3.27) into Eq. (3.24), and considering the local rest frame of the fluid, we arrive at the bosonic part of the shear viscosity from Eq. (3.26). To perform the p integration in Eq. (3.26) and study eventually the T dependence of η_b, the p and T dependence of E_b and Γ_b are to be determined perturbatively in an appropriate loop expansion in orders of the Yukawa coupling. In this paper, we will approximate $E_b \simeq \omega_b$ and will determine in Sec. IV only Γ_b at the one-loop level. The result will eventually be used to determine the T dependence of η_b. As concerns the μ dependence of η_b, we will use the same relation, Eq. (3.26). In this case, the μ dependence of η_b arises only from Γ_b on the rhs of Eq. (3.26).

B. The fermionic contribution to η in the one-loop skeleton expansion

To determine the fermionic part of the shear viscosity η_f, we will follow the same steps as in the previous section, and will present η_f in terms of fermionic spectral widths $\Gamma_\pm$, corresponding to normal and collective excitations of fermions. The resulting expression builds the central analytical result of the present paper.

To start, let us first consider Eq. (3.9). Using the standard Källen-Lehmann representation, the fermionic two-point Green's function $S_T(\mathbf{p},\omega_n)$ can be given in terms of the fermionic spectral density function $\rho_f(\mathbf{p},\omega)$ as

$$S_T(\mathbf{p},\omega_n) = \frac{1}{2\pi}\int_{-\infty}^{+\infty}d\omega\frac{\rho_f(\mathbf{p},\omega)}{\omega + i\omega_n}. \tag{3.28}$$

Plugging this relation into

$$S_T(\mathbf{p},\tau)=T\sum_{n=-\infty}^{+\infty}e^{-i\omega_n\tau}S_T(\mathbf{p},\omega_n),\qquad(3.29)$$

and adding over fermionic Matsubara frequencies $\omega_n=(2n+1)\pi T$, we arrive at

$$S_T(\mathbf{p},\tau)=\frac{1}{2\pi}\int_{-\infty}^{+\infty}d\omega e^{-\omega\tau}\rho_f(\mathbf{p},\omega)\times[\theta(\tau)(1-n_f(\omega))-\theta(-\tau)n_f(\omega)],\qquad(3.30)$$

with the fermionic distribution function

$$n_f(\omega)=\frac{1}{e^{\beta\omega}+1}.\qquad(3.31)$$

Plugging $S_T(\mathbf{p},\tau)$ from Eq. (3.30) into Eq. (3.9), and integrating over τ, using

$$\begin{aligned}&\int_0^\beta d\tau e^{(i\omega_n-\omega_1+\omega_2)\tau}\\&\quad\times[\theta(\tau)(1-n_f(\omega_1))-\theta(-\tau)n_f(\omega_1)]\\&\quad\times[\theta(-\tau)(1-n_f(\omega_2))-\theta(\tau)n_f(\omega_2)]\\&=\frac{(1-n_f(\omega_1))n_f(\omega_2)-(1-n_f(-\omega_1))n_f(-\omega_2)}{i\omega_n-\omega_1+\omega_2},\end{aligned}\qquad(3.32)$$

we arrive first at

$$\begin{aligned}\Pi_T^f(\omega_n)=&\frac{1}{2\pi^2}\int\frac{d^3p}{(2\pi)^3}\eta^{\alpha\beta\rho\sigma}p_\rho p_\sigma\\&\times\int d\omega_1d\omega_2(1-n_f(\omega_1))n_f(\omega_2)\\&\times\left\{\frac{\mathrm{tr}(\rho_f(\omega_1,\mathbf{p})\gamma_\alpha\rho_f(\omega_2,\mathbf{p})\gamma_\beta)}{i\omega_n-\omega_1+\omega_2}\right.\\&\left.-\frac{\mathrm{tr}(\rho_f(-\omega_1,-\mathbf{p})\gamma_\alpha\rho_f(-\omega_2,-\mathbf{p})\gamma_\beta)}{i\omega_n+\omega_1-\omega_2}\right\},\end{aligned}\qquad(3.33)$$

where $\eta^{\alpha\beta\rho\sigma}$ is defined below Eq. (3.6). To evaluate $\Pi_T(\omega_n)$, let us use at this stage, in analogy to the bosonic case, the definition of the fermionic spectral density function ρ_f in terms of the retarded two-point Green's function S_R,

$$\rho_f(p)=-2\mathfrak{Im}[S_R(p)],\qquad(3.34)$$

and the decomposition of $S_R(p)$ in terms of the fermion self-energy Σ_R^f,

$$S_R^{-1}(p)=\gamma\cdot p-m_f+\Sigma_R^f(p).\qquad(3.35)$$

Using the method, described in detail in Appendix A, the spectral density function of fermions is given by

$$\begin{aligned}\rho_f(\mathbf{p},\omega)=&\frac{2\Gamma_+(\mathbf{p},\omega_f)}{[\omega-E_+(\mathbf{p},\omega_f]^2+\Gamma_+^2(\mathbf{p},\omega_f)}\hat{g}_+(\mathbf{p},\omega_f)\\&-\frac{2\Gamma_-(\mathbf{p},\omega_f)}{[\omega+E_-(\mathbf{p},\omega_f)]^2+\Gamma_-^2(\mathbf{p},\omega_f)}\hat{g}_-(\mathbf{p},\omega_f),\end{aligned}\qquad(3.36)$$

where $\omega_f^2=\mathbf{p}^2+m_f^2$, and

$$\hat{g}_\pm(\mathbf{p},\omega_f)=\frac{1}{2\omega_f}[\gamma_0\omega_f\mp(\gamma.\mathbf{p}-m_f)].\qquad(3.37)$$

In Eq. (3.36), $E_\pm$ and $\Gamma_\pm$ are defined by [see Appendix A for more details]

$$\begin{aligned}E_\pm(\mathbf{p},\omega_f)&\equiv\omega_f\pm\frac{1}{2}\mathrm{tr}(\hat{g}_\pm(\mathbf{p},\omega_f)\mathfrak{Re}[\Sigma_R^f(\mathbf{p},\omega_f)]),\\\Gamma_\pm(\mathbf{p},\omega_f)&\equiv\pm\frac{1}{2}\mathrm{tr}(\hat{g}_\pm(\mathbf{p},\omega_f)\mathfrak{Im}[\Sigma_R^f(\mathbf{p},\omega_f)]).\end{aligned}\qquad(3.38)$$

In Ref. [29], almost the same expression for ρ_f as in Eq. (3.36) was introduced. However, in contrast to Eq. (3.36), only one spectral width for the fermion appears in the relation presented in Ref. [29]. Apparently, $\Gamma_+\simeq\Gamma_-$ is assumed. In what follows, we do not make this approximation, and after deriving η_f in terms of $\Gamma_\pm$, we will explore the effect of Γ_+ and Γ_- on the thermal properties of η_f. Let us notice at this stage, that the plus and minus signs appearing on $E_\pm$ and $\Gamma_\pm$ correspond to the normal and collective (plasmino) modes of the fermions [25]. In the chiral limit $m_f\to0$, they correspond to the same and opposite helicity and chirality of massless fermions, respectively [26].

Let us now consider Eq. (3.33), which will be simplified in what follows. Using the symmetry properties of $E_\pm(p)$ and $\Gamma_\pm(p)$,

$$\begin{aligned}E_\pm(\mathbf{p},-\omega_f)&=-E_\pm(\mathbf{p},\omega_f),\\\Gamma_\pm(\mathbf{p},-\omega_f)&=+\Gamma_\pm(\mathbf{p},\omega_f),\end{aligned}\qquad(3.39)$$

which we could verify only at the one-loop level, we obtain

$$\begin{aligned}\rho_f(-\mathbf{p},-\omega)=&\rho_f(\mathbf{p},\omega)\\&-\frac{2m_f}{\omega_f}\left\{\frac{\Gamma_+(\mathbf{p},\omega_f)}{[\omega-E_+(\mathbf{p},\omega_f)]^2+\Gamma_+^2(\mathbf{p},\omega_f)}\right.\\&\left.+\frac{\Gamma_-(\mathbf{p},\omega_f)}{[\omega+E_-(\mathbf{p},\omega_f)]^2+\Gamma_-^2(\mathbf{p},\omega_f)}\right\}.\end{aligned}\qquad(3.40)$$

Using Eq. (3.40) together with the properties of the traces of Dirac γ matrices, we have

$$\begin{aligned}&\mathrm{tr}(\rho_f(-\mathbf{p},-\omega_1)\gamma_\alpha\rho_f(-\mathbf{p},-\omega_2)\gamma_\beta)\\&\quad=\mathrm{tr}(\rho_f(\mathbf{p},\omega_1)\gamma_\alpha\rho_f(\mathbf{p},\omega_2)\gamma_\beta).\end{aligned}\qquad(3.41)$$

Now, by implementing this relation in Eq. (3.33), we arrive after analytical continuation, $i\omega_n \to p_0 + i\epsilon$, at

$$\Pi_R^f(p_0) = \frac{1}{2\pi^2}\int \frac{d^3p}{(2\pi)^3}\eta^{\alpha\beta\rho\sigma}p_\rho p_\sigma \times \int_{-\infty}^{+\infty} d\omega_1 d\omega_2 \mathrm{tr}(\rho_f(\omega_1,\mathbf{p})\gamma_\alpha\rho_f(\omega_2,\mathbf{p})\gamma_\beta) \times (1-n_f(\omega_1))n_f(\omega_2)W_\epsilon(\bar{\omega}_{12},p_0), \quad (3.42)$$

where $\bar{\omega}_{12} \equiv \omega_1 - \omega_2$ and W_ϵ is defined in Eq. (3.17). To derive the fermionic part of the shear viscosity η_f from Eq. (2.15), we follow the same steps as in the previous section for the bosonic case. Plugging Eq. (3.36) into Eq. (3.42), and after performing a straightforward mathematical computation, where mainly the relations

$$\frac{i}{10}\frac{d}{dp_0}W_\epsilon(p_0,\bar{\omega}_{12})|_{p_0=0} = -\frac{\pi}{5}\delta'(\bar{\omega}_{12}), \quad (3.43)$$

and

$$\mathrm{tr}(\hat{g}_\pm\gamma_\alpha\hat{g}_\mp\gamma_\rho) = \frac{1}{\omega_f^2}\{2\omega_f^2(g_{0\alpha}g_{0\rho} - g_{\alpha\rho}) - p_i p_j(g_\alpha^i g_\rho^j + g_\rho^i g_\alpha^j)\}.$$

$$\mathrm{tr}(\hat{g}_\pm\gamma_\alpha\hat{g}_\pm\gamma_\rho) = \frac{1}{\omega_f^2}\{2\omega_f^2 g_{0\alpha}g_{0\rho} \mp 2\omega_f p_i(g_\alpha^0 g_\rho^i + g_\rho^0 g_\alpha^i) + p_i p_j(g_\alpha^i g_\rho^j + g_\rho^i g_\alpha^j)\}, \quad (3.44)$$

in the local rest frame of the fluid are used, we arrive at

$$\eta_f = \frac{8\beta}{15\pi}\int\frac{d^3p}{(2\pi)^3}\int_{-\infty}^{+\infty} d\omega F_f(\mathbf{p},\omega), \quad (3.45)$$

with

$$F_f(\mathbf{p},\omega) \equiv \frac{e^{\beta\omega}}{(e^{\beta\omega}+1)^2}\mathbf{p}^2\left\{\frac{\mathbf{p}^2}{\omega_f^2}\left(\frac{\Gamma_+}{(\omega-E_+)^2+\Gamma_+^2} + \frac{\Gamma_-}{(\omega+E_-)^2+\Gamma_-^2}\right)^2 - \frac{2\Gamma_+\Gamma_-}{[(\omega-E_+)^2+\Gamma_+^2][(\omega+E_-)^2+\Gamma_-^2]}\right\}, \quad (3.46)$$

where $\omega \equiv \frac{1}{2}\omega_{12} = \frac{1}{2}(\omega_1 - \omega_2)$, and $E_\pm = E_\pm(\mathbf{p},\omega_f)$ as well as $\Gamma_\pm = \Gamma_\pm(\mathbf{p},\omega_f)$ are defined in Eq. (3.38). To evaluate the integration over ω in Eq. (3.46), the pole structure of $F_f(\mathbf{p},\omega)$ is to be considered. Similar to the previous case of bosonic fields, the contributions of the poles arising from the denominator $e^{\beta\omega}+1$ in Eq. (3.46) turn out to be proportional to $\Gamma_\pm^2$, and, assuming that Γ_+ and Γ_- are small enough, they can be neglected. As concerns the residue of the remaining poles, we have to close the contour in the upper half-plane and consider only two residues $\omega^\pm \equiv \pm E_\pm + i\Gamma_\pm$. Expanding the resulting expression in a Laurent series in orders of $\Gamma_\pm$, and using

$$\int_{-\infty}^{+\infty} d\omega \frac{e^{\beta\omega}}{(e^{\beta\omega}+1)^2}\frac{\Gamma_\pm^2}{[(\omega\mp E_\pm)^2+\Gamma_\pm^2]^2} \approx \pi\frac{e^{\beta E_\pm}}{(e^{\beta E_\pm}+1)^2}\frac{1}{2\Gamma_\pm},$$

$$\int_{-\infty}^{+\infty} d\omega \frac{\Gamma_+\Gamma_-}{[(\omega-E_+)^2+\Gamma_+^2][(\omega+E_-)^2+\Gamma_-^2]} \approx \pi\sum_{s=\pm}\frac{e^{\beta E_s}}{(e^{\beta E_s}+1)^2}\frac{\Gamma_f^+ - \Gamma_s}{[E_f + is\Gamma_f^+][E_f + i\Gamma_f^-]}, \quad (3.47)$$

where

$$E_f \equiv E_+ + E_-, \qquad \Gamma_f^\pm \equiv \Gamma_+ \pm \Gamma_-, \quad (3.48)$$

we arrive, after performing the integration over three-dimensional angles in Eq. (3.45), at the fermionic part of the shear viscosity of the Yukawa theory,

$$\eta_f = \frac{2\beta}{15\pi^2}\int_0^\infty dp\frac{\mathbf{p}^4}{\omega_f^2}\sum_{s=\pm}\left\{\frac{e^{\beta E_s}}{(e^{\beta E_s}+1)^2} \times\left[\frac{\mathbf{p}^2}{\Gamma_s} - \frac{4m_f^2(\Gamma_f^+ - \Gamma_s)}{[E_f + is\Gamma_f^+][E_f + i\Gamma_f^-]}\right]\right\} + \mathcal{O}(\Gamma_\pm^0). \quad (3.49)$$

Here, $E_f = E_f(\mathbf{p},\omega_f)$, $\Gamma_\pm = \Gamma_\pm(\mathbf{p},\omega_f)$ and $\Gamma_f^\pm = \Gamma_f^\pm(\mathbf{p},\omega_f)$ are defined in Eqs. (3.38) and (3.48). Let us notice that the first term of the above relation for η_f is comparable with the shear viscosity corresponding to fermions appearing in Ref. [9] in a relaxation-time approximation. Moreover, it resembles the η_f presented recently in Ref. [19]. There, the authors expressed η_f first in terms of the fermionic density function, ρ_f, which in contrast to Eq. (3.36), possessed a generalized Breit-Wigner shape, including only a quasiparticle mass M and a fermionic width Γ_f. Using this ansatz for ρ_f, they then arrived at η_f in this quasiparticle approximation [see Eq. (22) in Ref. [19]]. We, however, will work with Eq. (3.49) and after determining $\Gamma_\pm$ in a one-loop perturbative expansion, in the next section, will study the thermal properties of $\eta_f[\Gamma_\pm]$ for various masses m_b and m_f. We will then determine the difference between $\eta_f[\Gamma_+ = \Gamma_-]$ and $\eta_f[\Gamma_+ \neq \Gamma_-]$. In Appendix C, we generalize the method presented in this section for the case of nonvanishing chemical potential. We will show that in this case Eq. (C1), replaces Eq. (3.49), and can be used to explore the thermal properties of η_f at finite T and μ.

IV. PERTURBATIVE COMPUTATION OF BOSONIC AND FERMIONIC SPECTRAL WIDTHS

In this section, we will perturbatively compute the bosonic and fermionic spectral widths of the Yukawa theory from Eqs. (3.20) and (3.38) at the one-loop level. To do this, the imaginary part of the one-loop bosonic and fermionic self-energy diagrams will be evaluated using the standard Schwinger-Keldysh real-time formalism [36]. In what follows, we will closely follow the notations of Refs. [37] and [38]. According to this formalism, the free propagator of scalar bosons is given by

$$\mathcal{G} = \begin{pmatrix} G_{++} & G_{+-} \\ G_{-+} & G_{--} \end{pmatrix}, \tag{4.1}$$

where $G_{ab}, a, b = \pm$ read

$$\begin{aligned} G_{++}(p) &= -\frac{i}{p^2 - m_b^2 + i\epsilon} - 2\pi n_b(|p_0|)\delta(p^2 - m_b^2), \\ G_{+-}(p) &= -2\pi[\theta(-p_0) + n_b(|p_0|)]\delta(p^2 - m_b^2), \\ G_{-+}(p) &= -2\pi[\theta(p_0) + n_b(|p_0|)]\delta(p^2 - m_b^2), \\ G_{--}(p) &= \frac{i}{p^2 - m_b^2 - i\epsilon} - 2\pi n_b(|p_0|)\delta(p^2 - m_b^2). \end{aligned} \tag{4.2}$$

Here, m_b is the boson mass and $n_b(p_0)$ is the bosonic distribution function defined in Eq. (3.15). Similarly, the free fermion propagator is given by

$$\mathcal{S} = \begin{pmatrix} S_{++} & S_{+-} \\ S_{-+} & S_{--} \end{pmatrix}, \tag{4.3}$$

with the components

$$\begin{aligned} S_{++}(p) &= (\gamma \cdot p + m_f)\left(-\frac{i}{p^2 - m_f^2 + i\epsilon} + 2\pi n_f(|p_0|)\delta(p^2 - m_f^2)\right), \\ S_{+-}(p) &= -2\pi(\gamma \cdot p + m_f)[\theta(-p_0) - n_f(|p_0|)]\delta(p^2 - m_f^2), \\ S_{-+}(p) &= -2\pi(\gamma \cdot p + m_f)[\theta(p_0) - n_f(|p_0|)]\delta(p^2 - m_f^2), \\ S_{--}(p) &= (\gamma \cdot p + m_f)\left(\frac{i}{p^2 - m^2 - i\epsilon} + 2\pi n_f(|p_0|)\delta(p^2 - m_f^2)\right). \end{aligned} \tag{4.4}$$

Here, m_f is the fermion mass and $n_f(p_0)$ is the fermionic distribution function defined in Eq. (3.31). Combining $G_{ab}, a, b = \pm$ and $S_{ab}, a, b = \pm$, the physical retarded (R) and advanced (A) two-point Green's functions for scalar bosons, $G_{R/A}$, and fermions, $S_{R/A}$, are given by

$$G_R = G_{++} + G_{+-}, \qquad G_A = G_{++} + G_{-+}, \tag{4.5}$$

and

$$S_R = S_{++} + S_{+-}, \qquad S_A = S_{++} + S_{-+}. \tag{4.6}$$

To determine the spectral widths, Γ_b and $\Gamma_\pm$ from Eqs. (3.20) and (3.38), the imaginary parts of the bosonic and fermionic one-loop self-energies, Σ_R^b and Σ_R^f, are to be computed. In the real-time formalism, this is done using the finite-temperature cutting rules [37,38]. The main ingredients of these rules are specific propagators and vertices, which for the Yukawa theory, are demonstrated in Fig. 2. Here, $G_{ab}^{\pm}$ and $S_{ab}^{\pm}$ with $a, b = \pm$ are the retarded $(+)$ and advanced $(-)$ part of the bosonic and fermionic Green's functions. They are defined in the following decomposition for a generic Green's function, $\mathcal{D}_{ab}$, with $a, b = \pm$:

$$\mathcal{D}_{ab}(x) = \theta(t)\mathcal{D}_{ab}^{+}(x) + \theta(-t)\mathcal{D}_{ab}^{-}(x). \tag{4.7}$$

Using the definitions $\mathcal{D}_{ab}, a, b = \pm$ and $\mathcal{D} = \{G, S\}$, from Eqs. (4.2) and (4.4), we get the following identities:

$$\begin{aligned} \mathcal{D}_{++}^{+} &= \mathcal{D}_{--}^{-} = \mathcal{D}_{-+}^{+} = \mathcal{D}_{-+}^{-} = \mathcal{D}_{-+}, \\ \mathcal{D}_{++}^{-} &= \mathcal{D}_{--}^{+} = \mathcal{D}_{+-}^{+} = \mathcal{D}_{+-}^{-} = \mathcal{D}_{+-}. \end{aligned} \tag{4.8}$$

In what follows, we will separately compute the imaginary part of the one-loop self-energy corrections to bosonic and

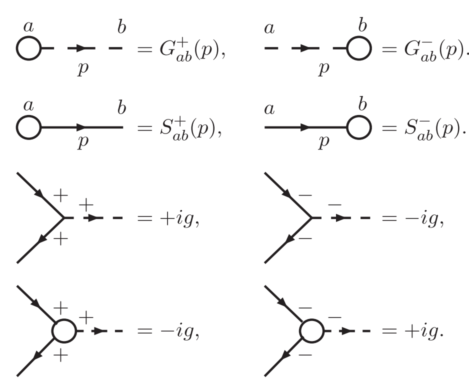

FIG. 2. Feynman rules that are necessary to compute the imaginary part of the bosonic and fermionic one-loop self-energy diagrams of the Yukawa theory (see Figs. 3 and 4). The definitions of $G_{ab}^{\pm}$ and $S_{ab}^{\pm}$ with $a, b = \pm$ in terms of G_{ab} and S_{ab} from Eqs. (4.2) and (4.4) are presented in Eq. (4.8).

fermionic two-point Green's functions. The results will eventually be used to determine the bosonic and fermionic spectral widths.

A. Bosonic spectral width in the one-loop perturbative expansion

Let us consider the bosonic spectral width Γ_b from Eq. (3.20), which when evaluated at $\omega_b = (\mathbf{p}^2 + m_b^2)^{1/2}$ reads

$$\Gamma_b(\mathbf{p}, \omega_b) = -\frac{1}{2\omega_b} \mathfrak{Im}[\Sigma_R^b(\mathbf{p}, \omega_b)]. \tag{4.9}$$

To determine the imaginary part of $\Sigma_R^b(p)$ at the one-loop level, we will use the diagrammatic representation of the cutting rules [37,38], demonstrated in Fig. 3. Using the propagators and vertices presented in Fig. 2, the imaginary part of $\Sigma_R^b(p)$ reads

$$\mathfrak{Im}[\Sigma_R^b(p)] = -\frac{g^2}{2} \int \frac{d^4k}{(2\pi)^4} \mathrm{tr}(S_{++}^-(k-p) S_{++}^+(k) - S_{-+}^-(k-p) S_{+-}^+(k)), \tag{4.10}$$

where, according to Eq. (4.7) with $\mathcal{D}_{ab} = S_{ab}$, S_{ab}^+ and S_{ab}^- are the retarded and advanced parts of the fermionic Green's function $S_{ab}, a, b = \pm$ from Eq. (4.4), respectively. To derive the spectral width of bosons, we use the identities (4.8) together with Eq. (4.4), and—after performing the integration over k_0 and some straightforward manipulations first—arrive at

$$\begin{aligned}\Gamma_b(\mathbf{p}, \omega_b) = \frac{g^2}{8\omega_b} \int \frac{d^3k}{(2\pi)^2} \frac{(4m_f^2 - m_b^2)}{\omega_1\omega_2} &\times \{\delta(\omega_b - \omega_1 - \omega_2)[1 - n_f(\omega_1) - n_f(\omega_2)] \\ &+ \delta(\omega_b - \omega_1 + \omega_2)[n_f(\omega_1) - n_f(\omega_2)] \\ &- \delta(\omega_b + \omega_1 - \omega_2)[n_f(\omega_1) - n_f(\omega_2)] \\ &- \delta(\omega_b + \omega_1 + \omega_2)[1 - n_f(\omega_1) - n_f(\omega_2)]\}.\end{aligned} \tag{4.11}$$

Here, $\omega_1^2 \equiv \mathbf{k}^2 + m_f^2$ and $\omega_2^2 \equiv (\mathbf{k} - \mathbf{p})^2 + m_f^2$. The factor $(4m_f^2 - m_b^2)$ on the rhs of Eq. (4.11) arises by considering the on-mass-shell relations, $k^2 = m_f^2$ and $(k-p)^2 = m_f^2$ from the Dirac δ functions, appearing in S_{ab} from Eq. (4.10), with $S_{ab}, a, b = \pm$ given in Eq. (4.4). Using now the definition of the fermionic distribution functions $n_f(\omega)$ from Eq. (3.31), we get

$$\begin{aligned}\Gamma_b(\mathbf{p}, \omega_b) = \frac{g^2}{16\omega_b} \int \frac{d^3k}{(2\pi)^2} \frac{\sinh(\frac{\beta\omega_b}{2})}{\cosh(\frac{\beta\omega_1}{2})\cosh(\frac{\beta\omega_2}{2})} &\times \frac{(4m_f^2 - m_b^2)}{\omega_1\omega_2} \{\delta(\omega_b - \omega_1 - \omega_2) \\ &- \delta(\omega_b - \omega_1 + \omega_2) - \delta(\omega_b + \omega_1 - \omega_2) \\ &+ \delta(\omega_b + \omega_1 + \omega_2)\}.\end{aligned} \tag{4.12}$$

Note that in the rest frame of the scalar bosons with $\mathbf{p} = 0$, only the first term on the rhs of Eq. (4.11), proportional to $\delta(\omega_b - \omega_1 - \omega_2)$ will contribute. It leads to $m_b \geq 2m_f$, as a constraint on the relation between bosonic and fermionic masses. Thus, keeping in mind that $\Gamma_b(\mathbf{p}, \omega_b)$ is Lorentz invariant, it is in general given by

$$\Gamma_b(\mathbf{p}, \omega_b) = \frac{g^2}{16\omega_b} \int \frac{d^3k}{(2\pi)^2} \frac{\sinh(\frac{\beta\omega_b}{2})}{\cosh(\frac{\beta\omega_1}{2})\cosh(\frac{\beta\omega_2}{2})} \times \frac{(4m_f^2 - m_b^2)}{\omega_1\omega_2} \delta(\omega_b - \omega_1 - \omega_2). \tag{4.13}$$

After performing the integration over k, using the method described in Appendix C, the bosonic part of the spectral width of the Yukawa theory, evaluated in a one-loop perturbative expansion, reads

$$\begin{aligned}\Gamma_b(\mathbf{p}, \omega_b) &= \frac{g^2 T}{16\pi} \frac{\gamma_b^2(\xi^2 - 4)}{\xi^2\sqrt{1 - \gamma_b^2}} \\ &\times \ln\left[\frac{1 + \cosh\frac{\kappa_b}{2}\left(1 + \frac{1}{\xi}\sqrt{(\xi^2 - 4)(1 - \gamma_b^2)}\right)}{1 + \cosh\frac{\kappa_b}{2}\left(1 - \frac{1}{\xi}\sqrt{(\xi^2 - 4)(1 - \gamma_b^2)}\right)}\right].\end{aligned} \tag{4.14}$$

Here, $\xi \equiv \frac{m_b}{m_f}$ and $\gamma_b \equiv \frac{m_b}{\omega_b}$, with $\omega_b^2 = \mathbf{p}^2 + m_b^2$. Moreover, $\kappa_b \equiv \omega_b/T$. In Appendix C, we generalize the result presented in Eq. (4.14) to the case of nonvanishing chemical potential, μ. In this case, the one-loop contribution to the bosonic spectral width is presented in Eq. (C14).

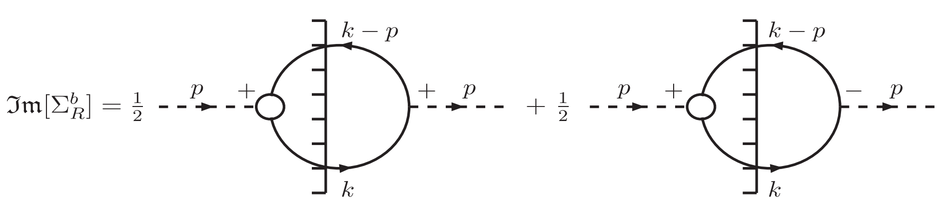

FIG. 3. Diagrammatic representation of the cutting rules leading to the imaginary part of the retarded part of the one-loop self-energy diagram for scalar bosons, Σ_R^b in the Yukawa theory.

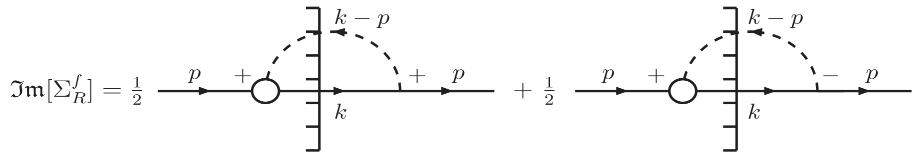

FIG. 4. Diagrammatic representation of the cutting rules leading to the imaginary part of the retarded part of the one-loop self-energy diagram for fermions, Σ_R^f in the Yukawa theory.

In Sec. V, we will use Eqs. (4.14) and (C14) to study the thermal properties of Γ_b. Eventually Γ_b will be inserted into Eq. (3.26) and the thermal properties of η_b for various ξ will be studied.

B. Fermionic spectral width in the one-loop perturbative expansion

As we have demonstrated in the previous section, fermions possess two different spectral widths $\Gamma_\pm$, defined in Eq. (3.38). They can be perturbatively computed by evaluating the imaginary part of the retarded fermion self-energy Σ_R^f in an appropriate loop expansion. In what follows, in analogy to the bosonic case, the standard finite-temperature cutting rules from Refs. [37,38] will be used to evaluate the imaginary part of Σ_R^f at the one-loop level. Using the Feynman rules presented in Fig. 2, and the diagrammatic representation of $\mathfrak{Im}[\Sigma_R^f]$ demonstrated in Fig. 4, we arrive first at

$$\mathfrak{Im}[\Sigma_R^f(p)] = \frac{g^2}{2}\int\frac{d^4k}{(2\pi)^4}[S_{++}^{+}(k)G_{++}^{-}(k-p) - S_{+-}^{+}(k)G_{-+}^{-}(k-p)], \tag{4.15}$$

where $\mathcal{D}_{ab}^{\pm}, a, b=\pm$ and $\mathcal{D}_{ab}=\{G,S\}$ are defined in Eq. (4.7). Using the identities (4.8), with $\mathcal{D}=\{G,S\}$, together with the definitions of G_{ab} and $S_{ab}, a, b=\pm$ from Eqs. (4.2) and (4.4), we arrive after performing the integration over k_0 in Eq. (4.15) and some straightforward manipulations, at the fermionic spectral widths $\Gamma_\pm$, defined originally in Eq. (3.38),

$$\begin{aligned}\Gamma_\pm(\mathbf{p},\omega_f) = \pm\frac{g^2}{8\omega_f}\int\frac{d^3k}{(2\pi)^2}\frac{1}{\omega_1\omega_2}&[[\omega_f\omega_1\mp\mathbf{p}\cdot\mathbf{k}\pm m_f^2]\{\delta(\omega_f-\omega_1-\omega_2)[1-n_f(\omega_1)+n_b(\omega_2)]\\&+\delta(\omega_f-\omega_1+\omega_2)[n_f(\omega_1)+n_b(\omega_2)]\}+[\omega_f\omega_1\pm\mathbf{p}\cdot\mathbf{k}\mp m_f^2]\{\delta(\omega_f+\omega_1+\omega_2)[1-n_f(\omega_1)+n_b(\omega_2)]\\&+\delta(\omega_f+\omega_1-\omega_2)[n_f(\omega_1)+n_b(\omega_2)]\}].\end{aligned} \tag{4.16}$$

According to our notations from Fig. 4, $\omega_f^2\equiv\mathbf{p}^2+m_f^2$ corresponds to the momentum of the external fermion propagators, and $\omega_1^2\equiv k_0^2=\mathbf{k}^2+m_f^2$ and $\omega_2^2\equiv(k_0-p_0)^2=(\mathbf{k}-\mathbf{p})^2+m_b^2$ to the internal fermion and boson propagators, respectively. Here, in contrast to the bosonic case, only two terms on the rhs of Eq. (4.16), proportional to $\delta(\omega_f-\omega_1+\omega_2)$ and $\delta(\omega_f+\omega_1-\omega_2)$, contribute to the final results of Γ_+ and Γ_-. This is because of the specific kinematics of the $f\to bf$ process in the rest frame of the particles. Here, b and f correspond to a boson and a fermion, respectively. Thus, the fermionic spectral widths are determined after some algebraic manipulations, where the definitions (3.15) and (3.31) of bosonic and fermionic distribution functions are used. For Γ_+, we obtain

$$\begin{aligned}\Gamma_+(\mathbf{p},\omega_f) &= \frac{g^2}{32\omega_f}\int\frac{d^3k}{(2\pi)^2}\frac{(4m_f^2-m_b^2)}{\omega_1\omega_2}\frac{\cosh(\frac{\beta\omega_f}{2})}{\cosh(\frac{\beta\omega_1}{2})\sinh(\frac{\beta\omega_2}{2})}\\&\quad\times\{\delta(\omega_f-\omega_1+\omega_2)-\delta(\omega_f+\omega_1-\omega_2)\}.\end{aligned} \tag{4.17}$$

As concerns Γ_-, it is given, according to Eq. (3.48), by $\Gamma_-=\Gamma_+-\Gamma_f^-$, where Γ_f^- is given by

$$\begin{aligned}\Gamma_f^-(\mathbf{p},\omega_f) &= \frac{g^2}{8}\int\frac{d^3k}{(2\pi)^2\omega_2}\frac{\cosh(\frac{\beta\omega_f}{2})}{\cosh(\frac{\beta\omega_1}{2})\sinh(\frac{\beta\omega_2}{2})}\\&\quad\times\{\delta(\omega_f-\omega_1+\omega_2)+\delta(\omega_f+\omega_1-\omega_2)\}.\end{aligned} \tag{4.18}$$

Performing the integration over k in Eq. (4.17), and by making use of the method presented in Appendix B, Γ_+ reads

$$\begin{aligned}&\Gamma_+(\xi,\gamma_f,\kappa_f;T)\\&\quad=\frac{g^2T}{32\pi}\frac{\gamma_f^2(\xi^2-4)}{\sqrt{1-\gamma_f^2}}\\&\qquad\times\left\{\ln\left[\frac{1-\cosh(2\Xi_-)}{\cosh(\Upsilon_-+\Xi_+)-\cosh(\Upsilon_--\Xi_+)}\right]\right.\\&\qquad\left.-\ln\left[\frac{1+\cosh(2\Xi_--\kappa_f)}{\cosh(\Upsilon_-+\Xi_+)+\cosh(\Upsilon_+-\Xi_+)}\right]\right\}.\end{aligned} \tag{4.19}$$

Here, $\xi = \frac{m_b}{m_f}$ and $\gamma_f \equiv \frac{m_f}{\omega_f}$ with $\omega_f^2 = \mathbf{p}^2 + m_f^2$. Moreover, we have

$$\Xi_\pm = \frac{\kappa_f}{4}\xi\left[\xi \pm \sqrt{(\xi^2-4)(1-\gamma_f^2)}\right],$$
$$\Upsilon_\pm = \frac{\kappa_f}{2}(\gamma_f \pm 1), \tag{4.20}$$

with $\kappa_f \equiv \omega_f/T$. Similarly, the integration over k in Eq. (4.18) can be performed analytically. This is done in Appendix B, where the final result for Γ_f^- is presented in Eq. (B14). In Appendix C, the same method is used for the case of nonvanishing chemical potential and Γ_+ and Γ_f^- are determined at the one-loop level. The results for Γ_+ and Γ_f^- are presented in Eqs. (C17) and (C19), respectively.

In Sec. V, we will study the qualitative behavior of the dimensionless quantities Γ_+/g^2T and Γ_f^-/g^2T in terms of the dimensionless variables ξ, γ_f and κ_f. We will then study the T and μ dependence of Γ_+ and Γ_-, and will show that in a certain regime of the parameter space $\Gamma_f^- = \Gamma_+ - \Gamma_-$ is not negligible. Plugging the resulting expressions for $\Gamma_\pm$ and Γ_f^- into Eq. (3.49) and assuming that $E_f \sim \omega_f = (\mathbf{p}^2 + m_f^2)^{1/2}$, we will eventually explore the thermal properties of the fermionic part of the shear viscosity.

V. NUMERICAL RESULTS

In this section, we will mainly study the T and μ dependence of the bosonic and fermionic spectral widths Γ_b and $\Gamma_\pm$, as well as the thermal properties of the bosonic and fermionic parts of the shear viscosity, η_b and η_f. We will first determine the T and μ dependence of these quantities for constant $\xi_0 \equiv m_b^0/m_f^0$, including the T- and μ-independent bosonic and fermionic masses, m_b^0 and m_f^0, respectively. We then consider the standard thermal corrections of bosonic and fermionic masses [23], arising from standard HTL approximation,

$$(m_b^{\rm th})^2 = \frac{g^2}{6}\left(T^2 + \frac{3\mu^2}{\pi^2}\right),$$
$$(m_f^{\rm th})^2 = \frac{g^2}{16}\left(T^2 + \frac{\mu^2}{\pi^2}\right), \tag{5.1}$$

and will add these thermal corrections to the original constant m_b^0 and m_f^0. Using the definition

$$\xi(T,\mu) \equiv \frac{m_b(T,\mu)}{m_f(T,\mu)}, \tag{5.2}$$

with

$$m_b(T,\mu) \equiv m_b^0 + m_b^{\rm th}(T,\mu),$$
$$m_f(T,\mu) \equiv m_f^0 + m_f^{\rm th}(T,\mu), \tag{5.3}$$

we will then determine the T and μ dependence of $\Gamma_b, \Gamma_\pm$ as well as η_b and η_f, including the thermal corrections to bosonic and fermionic masses. According to the descriptions in Refs. [23,24], and since in the Yukawa theory the vertices do not receive any HTL corrections, the above treatment of thermal masses equals the HTL treatment with an approximate fermion propagator. In this way, the apparent drawback of our one-loop perturbative treatment of $\eta_b[\Gamma_b]$ and $\eta_f[\Gamma_\pm]$ is partly compensated. For the fermions, we mainly focus on the difference between Γ_+ and Γ_-, arising from normal and collective (plasmino) excitations of fermions at finite T and μ, respectively. In the literature, the spectral widths Γ_+ and Γ_- are often assumed to be equal (see e.g. Ref. [29]). We will show that depending on T and/or μ, their difference is not negligible. To study the effect of plasminos on η_f, we will determine η_f once for $\Gamma_+ \neq \Gamma_-$ and once for $\Gamma_+ = \Gamma_-$, and compare the corresponding results.

A. Bosonic contributions

1. Bosonic spectral width

Let us first consider Eqs. (4.14) and (C14), where the bosonic spectral width Γ_b is presented as a function of dimensionless parameters, $\gamma_b = \frac{m_b}{\omega_b}, \kappa_b = \omega_b/T$ with $\omega_b^2 = \mathbf{p}^2 + m_b^2$ and $\xi = \frac{m_b}{m_f}$ as well as $\tau_f = \mu/T$ for $\mu = 0$ [Eq. (4.14)] and $\mu \neq 0$ [Eq. (C14)]. We consider first the constant-mass approach, and replace all m_b and m_f with m_b^0 and m_f^0, respectively. We then focus on the ξ_0 dependence of Γ_b for fixed κ_b, γ_b and τ_f. In Fig. 5(a), the ξ_0 dependence of the dimensionless quantity $\frac{\Gamma_b}{g^2T}$ is plotted for $\tau_f = 0$ and $\kappa_b = 20$ as well as $\gamma_b = 0.5, 0.6, 0.7, 0.8$ [from bottom (red dashed line) to top (blue solid line)]. In Fig. 5(b), the ξ_0 dependence of $\frac{\Gamma_b}{g^2T}$ is plotted for $\tau_f = 0$ and $\gamma_b = 0.8$ as well as $\kappa_b = 1, 2, 3, 4$ [from bottom (red dashed line) to top (blue solid line)]. We observe that $\frac{\Gamma_b}{g^2T}$ remains constant for $\xi_0 \gtrsim 10$ in both cases. Moreover, for fixed values of ξ_0 and κ_b (γ_b), the ratio $\frac{\Gamma_b}{g^2T}$ increases with increasing γ_b (κ_b) [see panels (a) and (b) of Fig. 5].

In Fig. 6(a), the ξ_0 dependence of $\frac{\Gamma_b}{g^2T}$ is plotted for $\tau_f = 4$ and $\kappa_b = 20$ as well as $\gamma_b = 0.5, 0.6, 0.7, 0.8$ (from bottom to top). In Fig. 6(b), the same dimensionless quantity is plotted for $\tau_f = 4$ and $\gamma_b = 0.8$ as well as $\kappa_b = 1, 2, 3, 4$ (from bottom to top). Similar to the case of $\tau_f = 0$, $\frac{\Gamma_b}{g^2T}$ remains constant for $\xi_0 \gtrsim 10$, and increases with increasing $\gamma_b(\kappa_b)$ for fixed values of ξ_0 and κ_b (γ_b). In Fig. 6(c), the ξ_0 dependence of $\frac{\Gamma_b}{g^2T}$ is plotted for fixed $\kappa_b = 20$ and $\gamma_b = 0.8$ as well as $\tau_f = 4, 6, 8, 10$ [from top (red dashed line) to bottom (blue solid line)]. In contrast to the previous cases, $\frac{\Gamma_b}{g^2T}$ decreases with increasing τ_f and fixed κ_b, γ_b and ξ_0. These results indicate that Γ_b decreases with increasing T and/or μ. This conclusion is compatible with the observed

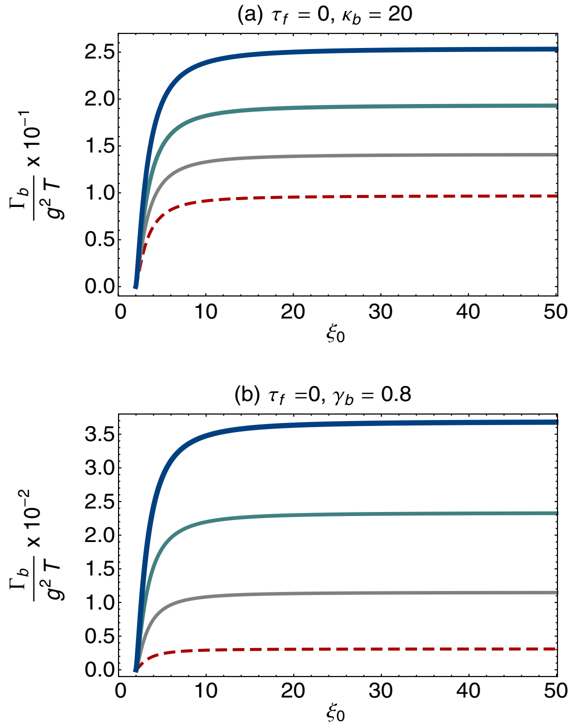

FIG. 5 (color online). The ξ_0 dependence of $\frac{\Gamma_b}{g^2T}$ for $\tau_f = 0$ and (a) $\kappa_b = 20$ as well as $\gamma_b = 0.5$, 0.6, 0.7, 0.8 (from bottom to top) and (b) $\gamma_b = 0.8$ as well as $\kappa_b = 1$, 2, 3, 4 (from bottom to top). As it turns out, $\frac{\Gamma_b}{g^2T}$ remains constant for $\xi_0 \gtrsim 10$. For fixed values of ξ_0 and κ_b (γ_b), $\frac{\Gamma_b}{g^2T}$ increases with increasing γ_b (κ_b) [see panel (b)].

result demonstrated in Figs. 7 and 8, where the T and μ dependence of Γ_b is studied for various fixed parameters.

In Fig. 7, the T dependence of Γ_b is plotted for $\omega_b = 300$ MeV, $m_f^0 = 5$ MeV and $\mu = 0$ MeV [Fig. 7(a)] as well as $\mu = 150$ MeV [Fig. 7(b)]. The Yukawa coupling is chosen to be $g = 0.5$. Similarly, in Fig. 8, the μ dependence of Γ_b is plotted for $\omega_b = 300, m_f^0 = 5$ MeV and $T = 10$ MeV [Fig. 8(a)] as well as $T = 100$ MeV [Fig. 8(b)]. The red, gray and blue lines in Figs. 7 and 8 correspond to $m_b^0 = 100, 150$ and 200 MeV, respectively. The dashed lines include the contributions of constant masses m_b^0 and m_f^0 for bosons and fermions, respectively, and the solid lines include the contributions of thermal corrections of fermion and boson masses, $m_b(T, \mu)$ and $m_f(T, \mu)$ from Eq. (5.3). As it turns out, Γ_b decreases with increasing T and μ. Having in mind that Γ_b^{-1} is essentially proportional to the mean free path of the bosons, λ_b [18], the fact that Γ_b decreases with increasing T and μ means that λ_b increases with increasing T and μ. However, for constant T and μ, heavier bosons seem to have smaller λ_b, as expected. Although, according to Figs. 7 and 8, adding T- and μ-dependent (thermal) masses of bosons and fermions to the bare masses m_b^0 and m_f^0 shifts Γ_b to larger values, but the qualitative interpretation concerning λ_b remains unchanged. According to Eq. (3.26), indicating that $\eta_b \sim \Gamma_b^{-1}$, the thermal behavior of λ_b is expected to be reflected in the thermal behavior of η_b, as it will be shown below.

2. Bosonic part of the shear viscosity

The bosonic part of the shear viscosity is presented in Eq. (3.26), with Γ_b given in Eq. (4.14) for $\mu = 0$ and in Eq. (C14) for $\mu \neq 0$. To determine η_b, we neglect the contribution of $\mathfrak{Re}[\Sigma_R^b(p)]$ in E_b from Eq. (3.19) and set $E_b \sim \omega_b$. In Fig. 9, the T dependence of η_b is plotted for $\mu = 0$. The black solid and red dashed lines in Fig. 9(a) correspond to the constant ratios $\xi_0 = 40$ MeV and $\xi_0 = 80$ MeV. The latter arises from $m_b^0 = 200, 400$ MeV and $m_f^0 = 5$ MeV, respectively. In Fig. 9(b), the T dependence of η_b is plotted for $\mu = 0$. But, in this case, in contrast to the plot in Fig. 9(a), η_b includes thermal masses $m_b(T, \mu)$ and $m_f(T, \mu)$ from Eq. (5.3) with $m_b^0 = 200, 400$ MeV and $m_f^0 = 5$ MeV. In Fig. 9(b), ξ_0^T denotes the ratio m_b^0/m_f^0 in $\xi(T, \mu)$ from Eq. (5.2). In Figs. 10(a) and (b), the same quantities are plotted for $\mu = 120$ MeV. Comparing the plots of η_b for different constant masses in Figs. 9(a) and 10(a), it turns out that η_b decreases with increasing ξ_0. The same is also true for $\xi(T, \mu)$ [see Figs. 9(b) and 10(b)]. These results are compatible with our findings in

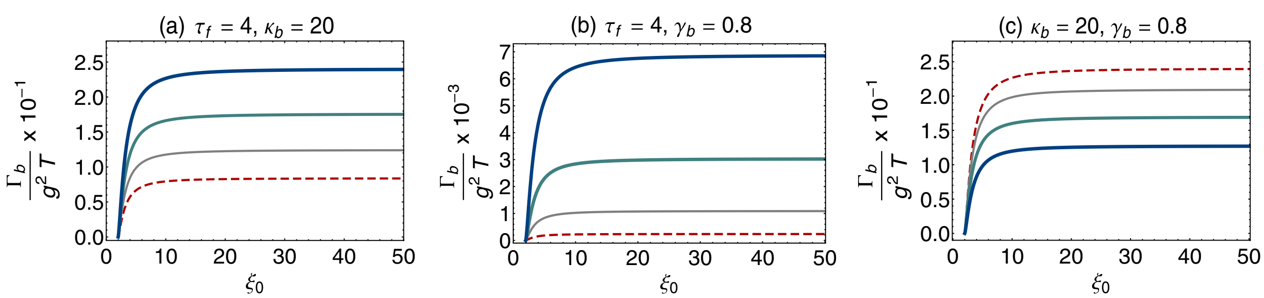

FIG. 6 (color online). The ξ_0 dependence of $\frac{\Gamma_b}{g^2T}$ for $\tau_f = 4$ and (a) $\kappa_b = 20$ as well as $\gamma_b = 0.5$, 0.6, 0.7, 0.8 (from bottom to top), and (b) $\gamma_b = 0.8$ as well as $\kappa_b = 1$, 2, 3, 4 (from bottom to top). As it turns out, $\frac{\Gamma_b}{g^2T}$ remains constant for $\xi_0 \gtrsim 10$. For a fixed value of ξ_0, $\frac{\Gamma_b}{g^2T}$ increases with increasing γ_b for all values of κ_b (panel a) and with increasing κ_b for all values of γ_b (panel b). (c) The ξ_0 dependence of $\frac{\Gamma_b}{g^2T}$ for fixed $\kappa_b = 20, \gamma_b = 0.8$ and $\tau_f = 4, 6, 8, 10$ (from top to bottom). As in the previous cases, $\frac{\Gamma_b}{g^2T}$ remains constant for $\xi_0 \gtrsim 10$ for all values of κ_b, γ_b and τ_f. For fixed values of κ_b, γ_b and ξ_0, $\frac{\Gamma_b}{g^2T}$ decreases with increasing τ_f.

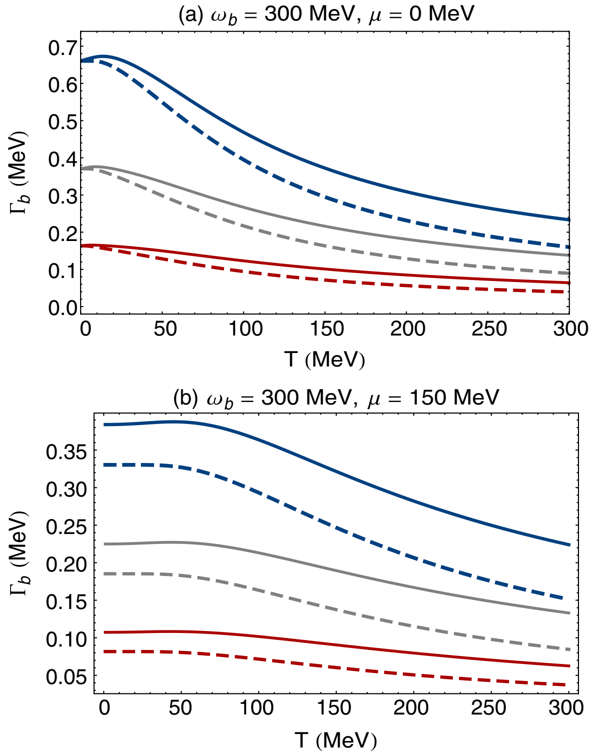

FIG. 7 (color online). The T dependence of Γ_b for $\omega_b = 300$ MeV and (a) $\mu = 0$ MeV as well as (b) $\mu = 150$ MeV. The red, gray and blue lines (from bottom to top) correspond to $m_b^0 = 100$, 150, 200 MeV and $m_f^0 = 5$ MeV, respectively. The dashed lines include only the constant-mass contributions of bosons, $m_b^0 = 100$, 150, 200 MeV, and fermions $m_f^0 = 5$ MeV. The solid lines include, in addition to the constant-mass contributions, the thermal corrections of the boson and fermion masses as functions of T and μ [see Eqs. (5.1)–(5.3)]. Here, the Yukawa coupling $g = 0.5$ is used.

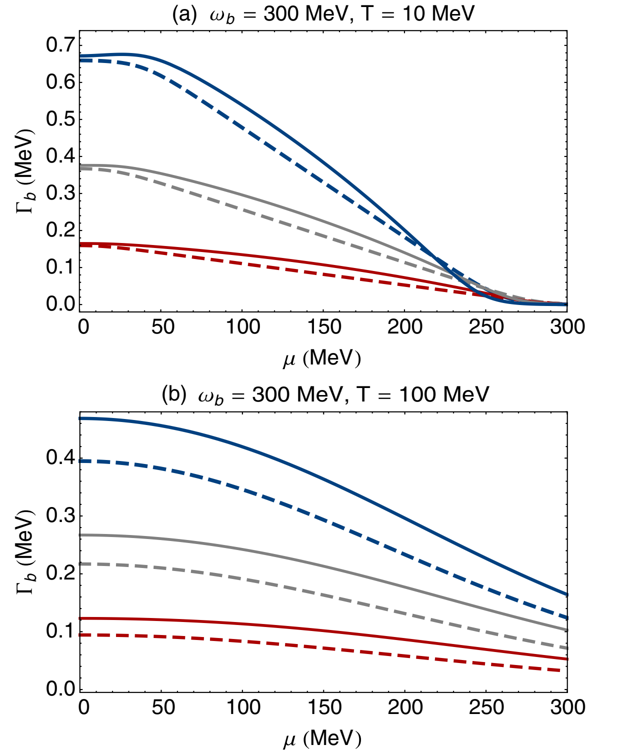

FIG. 8 (color online). The μ dependence of Γ_b for $\omega_b = 300$ MeV and (a) $T = 10$ MeV as well as (b) $T = 100$ MeV. The red, gray and blue lines (from bottom to top) correspond to $m_b^0 = 100$, 150, 200 MeV and $m_f^0 = 5$ MeV, respectively. The dashed lines include only the constant-mass contributions of bosons, $m_b^0 = 100$, 150, 200 MeV, and fermions, $m_f^0 = 5$ MeV. The solid lines include, in addition to the constant-mass contributions, the thermal corrections of the boson and fermion masses as functions of T and μ [see Eqs. (5.1)–(5.3)]. Here, the Yukawa coupling $g = 0.5$ is used.

Figs. 7(a) and 7(b), since for constant T and μ, η_b is approximately proportional to Γ_b^{-1} [see Eq. (3.26)]. Moreover, as expected from Fig. 7, η_b increases with increasing T. Comparing the results for constant and (T,μ)-dependent masses in Figs. 9 and 10, it turns out that, as expected from Fig. 7, adding the thermal corrections to the constant bosonic and fermionic masses decreases the value of η_b. Moreover, for both constant and T- or/and μ-dependent masses, the difference between η_b for different ξ_0 as well as ξ_0^T increases with increasing T. However, since the scales in the plots of Fig. 9 and Fig. 10 are different, the difference between η_b for ξ_0 and ξ_0^T seems to be negligible for the case $\mu \neq 0$ compared to the case $\mu = 0$. When we compare the plots of Fig. 9 with the plots of Fig. 10, it seems that η_b decreases with increasing μ. This conclusion contradicts the result from Figs. 7 and 8, together with the fact that $\eta_b \sim \Gamma_b^{-1}$ from Eq. (3.26). This apparent contradiction may lie in the fact that for $\mu \neq 0$, the p integration in Eq. (3.26) is taken in the interval $p \in [0, (\mu^2 - m_f^{02})^{1/2}]$ for the constant fermionic mass m_f^0, and $p \in [0, [\mu^2 - m_f^2(T,\mu)]^{1/2}]$, with the (T,μ)-dependent fermionic mass $m_f(T,\mu)$ from Eq. (5.3). Hence, the μ dependence of Γ_b is not the only source of the μ dependence of η_b. In Fig. 11, the μ dependence of η_b is demonstrated for constant $T = 120$ MeV and $\xi_0 = 40$ as well as (T,μ)-dependent $\xi(T,\mu)$ with $\xi_0^T = 40$. As expected from Figs. 7 and 8, η_b increases with increasing μ. Recently, in Ref. [39], the shear viscosity of a hot pion gas, η_π, was determined by solving the relativistic transport equation in the Chapman-Enskog and relaxation-time approximations. It is shown that for zero pion chemical potential, η_π increases with T. Although the setup discussed in Ref. [39] is slightly different from ours—the self-interaction of pseudoscalar pions is described by the Lagrangian density of chiral perturbation theory—our results for zero μ and finite T coincide with the results presented in Ref. [39]. Our results from Figs. 9–11—i.e. that η_b also increases with T or μ—show that T and μ have the same effect on the bosons propagating in a dissipative hot and dense medium. As we have argued in the previous

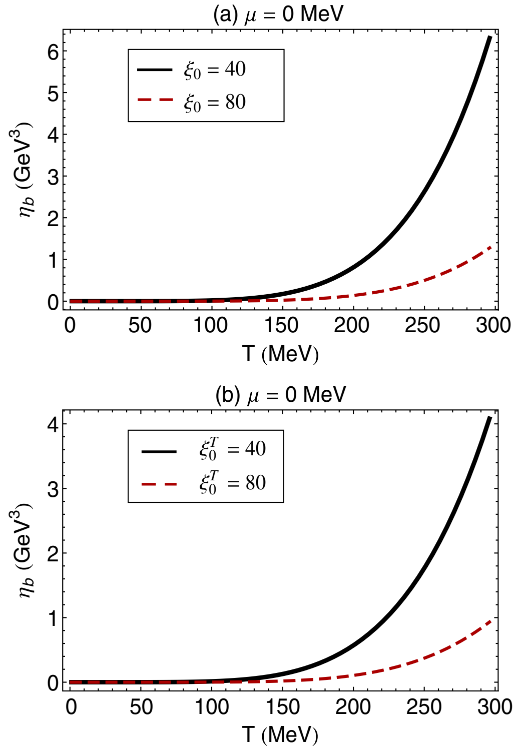

FIG. 9 (color online). (a) The T dependence of η_b is plotted for $\mu = 0$ and the T-independent $\xi_0 = 40, 80$ arising from $m_b^0 = 200, 400$ MeV and $m_f^0 = 5$ MeV. (b) The T dependence of η_b, including the T-dependent thermal corrections to bosonic and fermionic masses, is plotted for $m_b^0 = 200, 400$ MeV and $m_f^0 = 5$ MeV. Here, ξ_0^T denotes the ratio m_b^0/m_f^0 in $\xi(T,\mu)$ from Eqs. (5.2)–(5.3).

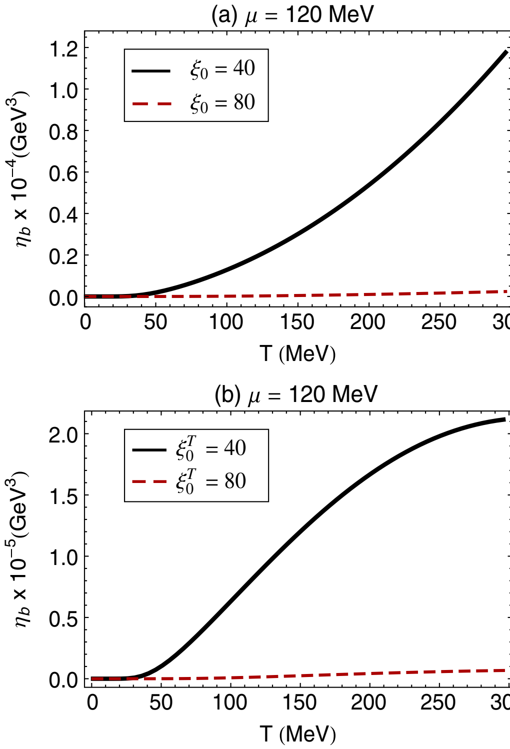

FIG. 10 (color online). (a) The T dependence of η_b is plotted for $\mu = 120$ MeV and (T,μ)-independent $\xi_0 = 40, 80$ arising from $m_b^0 = 200, 400$ MeV and $m_f^0 = 5$ MeV. (b) The T dependence of η_b, including the T- and μ-dependent thermal corrections to bosonic and fermionic masses, is plotted for $m_b^0 = 200, 400$ MeV and $m_f^0 = 5$ MeV, leading to $\xi_0^T = 40, 80$.

section, the mean free path of bosons, λ_b increases with increasing T and/or μ. The results of the present section show that the thermal properties of λ_b are directly reflected in the thermal properties of η_b. Moreover, as it turns out heavier bosons have smaller η_b and λ_b, as expected.

B. Fermionic contributions

1. Fermionic spectral width

In this section, we will focus on the T and μ dependence of the fermionic spectral widths $\Gamma_\pm$, with an emphasis on the difference between them. As aforementioned, in the chiral limit $m_f \to 0$ and at finite (T,μ), Γ_+ and Γ_- correspond to the normal and collective excitations of fermions, respectively. The latter is referred to as either a hole or a plasmino. Moreover, in the chiral limit, Γ_+ (Γ_-) corresponds to excitations with the same (opposite) chirality and helicity. The difference between Γ_+ and Γ_- is often neglected in the literature [29]. We, however, highlight this difference and study its impact on the fermionic shear viscosity in different regimes of temperature and chemical potential.

In Eqs. (4.19) and (C17), Γ_+ is presented for vanishing and nonvanishing μ in terms of the dimensionless parameters $\gamma_f = \frac{m_f}{\omega_f}, \kappa_f = \omega_f/T$ with $\omega_f^2 = \mathbf{p}^2 + m_f^2$ and $\xi = \frac{m_b}{m_f}$ as well as $\tau_f = \mu/T$. Similarly, $\Gamma_f^-(\gamma_f, \kappa_f, \tau_f; \xi)$ for $\mu = 0$ and $\mu \neq 0$ are presented in Eqs. (B14) and (C19), respectively. Using $\Gamma_- = \Gamma_+ - \Gamma_f^-$, Γ_- can be determined from the difference between Γ_+ and Γ_f^-. Similar to the bosonic case, let us replace m_b and m_f with (T,μ)-independent m_b^0 and m_f^0, respectively, and focus first on the $\xi_0 = m_b^0/m_f^0$ dependence of the dimensionless quantity $\frac{\Gamma_+}{g^2 T}$ as a function of the dimensionless parameters γ_f, κ_f and τ_f.

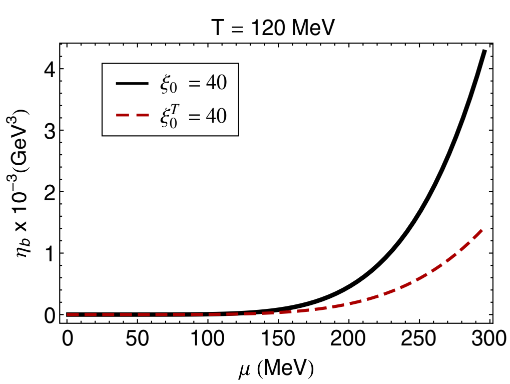

FIG. 11 (color online). The μ dependence of η_b is plotted for $T = 120$ MeV and $\xi_0 = \xi_0^T = 40$.

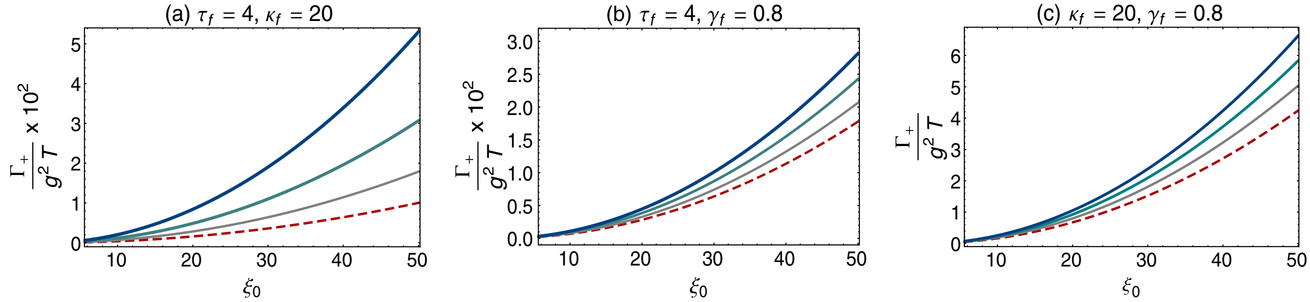

FIG. 12 (color online). The ξ_0 dependence of $\frac{\Gamma_+}{g^2T}$ for $\tau_f = 4$ and (a) $\kappa_f = 20$ as well as $\gamma_f = 0.5, 0.6, 0.7, 0.8$ (from bottom to top), and (b) $\gamma_f = 0.8$ as well as $\kappa_f = 2, 4, 6, 8$ (from bottom to top). (c) The ξ_0 dependence of $\frac{\Gamma_+}{g^2T}$ for $\kappa_f = 20, \gamma_f = 0.8$ and $\tau_f = 0, 3, 6, 9$ (from bottom to top). As it turns out, for a fixed ξ_0, $\frac{\Gamma_+}{g^2T}$ increases whenever one of the parameters γ_f, κ_f or τ_f increases and the other two parameters are held fixed. It can be shown that the same is also true for $\frac{\Gamma_-}{g^2T}$.

In Fig. 12(a), the ξ_0 dependence of $\frac{\Gamma_+}{g^2T}$ is plotted for fixed $\tau_f = 4$ and $\kappa_f = 20$ as well as $\gamma_f = 0.5, 0.6, 0.7, 0.8$ [from bottom (red dashed line) to top (blue solid line)]. Similarly, in Fig. 12(b), the ξ_0 dependence of $\frac{\Gamma_+}{g^2T}$ is plotted for $\tau_f = 4$ and $\gamma_f = 0.8$ as well as $\kappa_f = 2, 4, 6, 8$ [from bottom (red dashed line) to top (blue solid line)]. Finally, in Fig. 12(c), the ξ_0 dependence of $\frac{\Gamma_+}{g^2T}$ is plotted for fixed $\kappa_f = 20$ and $\gamma_f = 0.8$ as well as $\tau_f = 0, 3, 6, 9$ [from bottom (red dashed line) to top (blue solid line)]. In contrast to the bosonic case, for a fixed ξ_0, $\frac{\Gamma_+}{g^2T}$ increases whenever one of the parameters γ_f, κ_f or τ_f increases and the other two parameters are held fixed. Neglecting the tiny difference between $\frac{\Gamma_+}{g^2T}$ and $\frac{\Gamma_-}{g^2T}$, the same can easily be shown to be true for $\frac{\Gamma_-}{g^2T}$. Let us notice at this stage, that to derive the final results for $\Gamma_\pm$ for $\mu = 0$ and $\mu \neq 0$, the condition $m_b^0 \geq 2m_f^0$ was necessary. It is easy to show that $\Gamma_\pm$ diverges once $m_b^0 = m_f^0 = 0$. This was also indicated in Ref. [34], where it was noted that the nonzero boson and fermion mass difference, $\delta m^2 = m_b^2 - m_f^2$, ensures the smoothness of the fermion self-energy, and consequently $\Gamma_\pm$, in the far-infrared (IR) limit.

Although the ξ_0 dependence of $\frac{\Gamma_+}{g^2T}$ and $\frac{\Gamma_-}{g^2T}$ as functions of the dimensionless parameters γ_f, κ_f and τ_f are practically identical, the T (μ) dependence of Γ_+ and Γ_- turns out to be different for fixed values of μ (T) and ξ_0. In Figs. 13 and 14, the T and μ dependence of Γ_+ [panel (a)], Γ_- [panel (b)] and Γ_f^- [panel (c)] are plotted for $\omega_f = 300$ MeV and $\mu = 150$ MeV (Fig. 13), as well as for $\omega_f = 300$ MeV and $T = 150$ MeV (Fig. 14). The red, gray and blue solid and dashed lines correspond to $m_b^0 = 300, 450, 600$ MeV and $m_f^0 = 5$ MeV. The dashed lines correspond to $\Gamma_\pm$ and Γ_f^- as functions of the (T, μ)-independent $\xi_0 = 60, 90, 120$, and the solid lines correspond to the same quantities, including the thermal masses of bosons and fermions, with $\xi_0^T = m_b^0/m_f^0 = 60, 90, 120$. According to the results in Figs. 13 and 14, it turns out that the absolute value of the difference between Γ_+ and Γ_-, $|\Gamma_f^-|$, increases with increasing T and constant μ (Fig. 13), as well as with increasing μ and constant T (Fig. 14). It decreases

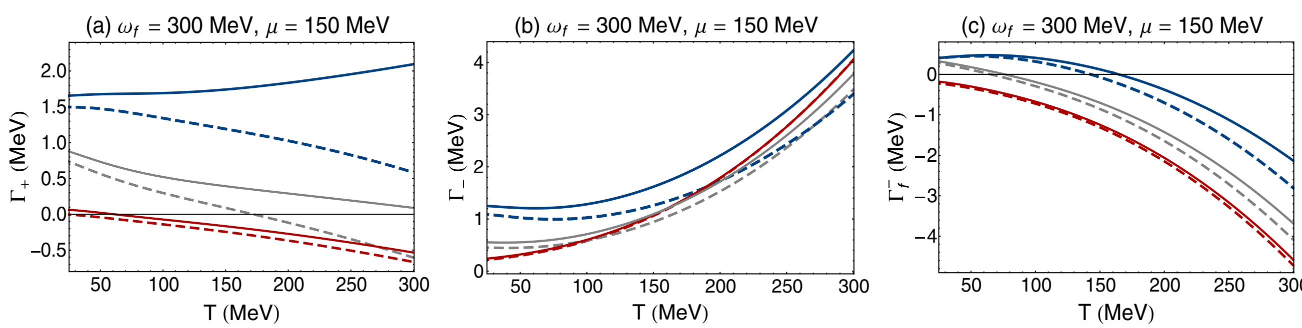

FIG. 13 (color online). The T dependence of (a) Γ_+, (b) Γ_- and (c) $\Gamma_f^- = \Gamma_+ - \Gamma_-$ is plotted for constant $\omega_f = 300$ MeV and $\mu = 150$ MeV. The red, gray and blue solid and dashed lines (from bottom to top) correspond to $m_b^0 = 300, 450, 600$ MeV and $m_f^0 = 5$ MeV. Whereas the dashed lines correspond to $\Gamma_\pm$ and Γ_f^- as functions of (T, μ)-independent $\xi_0 = 60, 90, 120$, the solid lines correspond to the same quantities including the thermal corrections to bosonic and fermionic masses with $\xi_0^T = 60, 90, 120$. It turns out that the absolute value of the difference between Γ_+ and Γ_-, i.e. $|\Gamma_f^-|$, increases with increasing T, and decreases with increasing ξ_0 and ξ_0^T. Moreover, for small ξ_0 or ξ_0^T and fixed (T, μ), Γ_- is always larger than Γ_+.

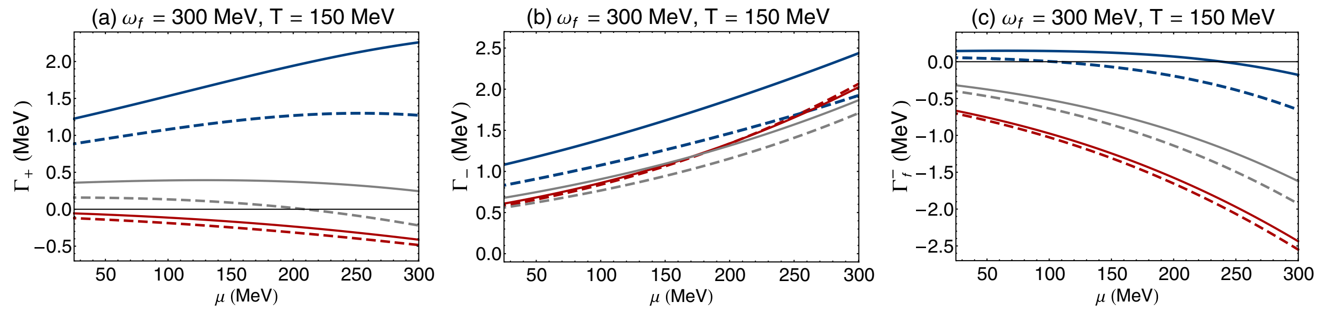

FIG. 14 (color online). The μ dependence of (a) Γ_+, (b) Γ_- and (c) $\Gamma_f^- = \Gamma_+ - \Gamma_-$ is plotted for constant $\omega_f = 300$ MeV and $T = 150$ MeV. The red, gray and blue solid and dashed lines (from bottom to top) correspond to $m_b^0 = 300, 450, 600$ MeV and $m_f^0 = 5$ MeV. Whereas the dashed lines correspond to $\Gamma_\pm$ and Γ_f^- as functions of the (T,μ)-independent $\xi_0 = 60, 90, 120$, the solid lines correspond to the same quantities including the thermal corrections to bosonic and fermionic masses with $\xi_0^T = 60, 90, 120$. Similar to their T dependence, demonstrated in Fig. 13, it turns out that $|\Gamma_f^-|$ increases with increasing μ, and decreases with increasing ξ_0 as well as ξ_0^T. Moreover, for small ξ_0 or ξ_0^T and fixed (T,μ), Γ_- is always larger than Γ_+.

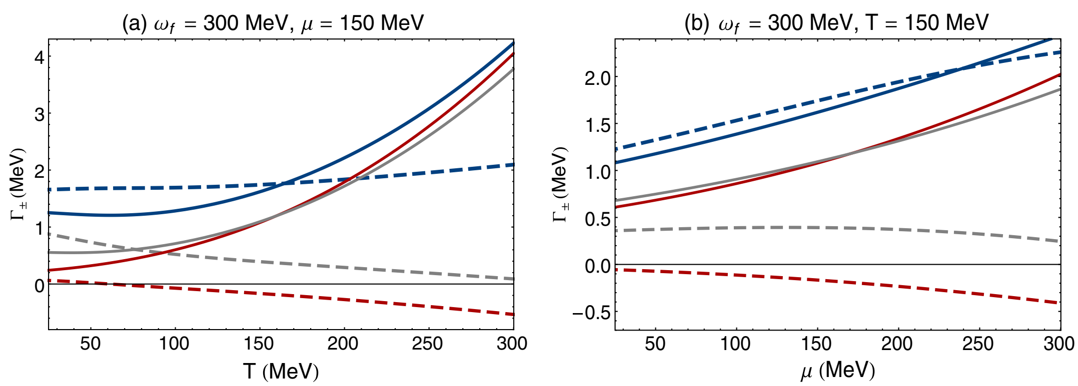

FIG. 15 (color online). (a) The T dependence of $\Gamma_\pm$ for $\omega_f = 300$ MeV and $\mu = 150$ MeV, including the thermal corrections to bosonic and fermionic masses. (b) The μ dependence of $\Gamma_\pm$ for $\omega_f = 300$ MeV and $T = 150$ MeV, including the thermal corrections to bosonic and fermionic masses. The dashed (solid) lines correspond to Γ_+ (Γ_-). The red, gray and blue dashed and solid lines (from bottom to top) correspond to $\xi_0^T = 60, 90$ and $\xi_0^T = 120$, respectively.

with increasing ξ_0 and ξ_0^T. Moreover, for small values of ξ_0 or ξ_0^T and fixed (T,μ), Γ_- is always larger than Γ_+.

To compare Γ_+ and Γ_- more directly, their T and μ dependence are plotted in Fig. 15 for constant $\omega_f = 300$ MeV and $\mu = 150$ MeV [panel (a)] and $T = 150$ MeV. Here, $\Gamma_\pm$ includes only thermal bosonic and fermionic masses. The dashed (solid) lines correspond to Γ_+ (Γ_-). The red, gray and blue dashed and solid lines correspond to $\xi_0^T = 60, 90, 120$, respectively. As it turns out, whereas for smaller $\xi_0^T = m_b^0/m_f^0$, Γ_+, the spectral width of normal fermion excitations, decreases with T or μ, for larger ξ_0^T, it increases with increasing T or μ. In contrast, Γ_-, the spectral width of the plasmino excitations, increases with T or μ, independent of ξ_0^T. Assuming, in analogy to the bosonic case, that the spectral widths Γ_+ and Γ_- are inversely proportional to the mean free paths of the normal and plasmino excitations of the fermions, λ_+ and λ_-, the above results suggest that at higher temperature or chemical potential, plasminos have smaller λ_-, while for normal fermions, the thermal behavior of λ_+ depends strongly on the relation between the masses of the fermions and bosons included in our Yukawa-Fermi gas. Heavier (normal) fermions have smaller λ_+, as expected. Let us mention that, according to the plots in Figs. 13 and 14, $|\Gamma_f^-| = |\Gamma_+ - \Gamma_-|$ increases with increasing T (μ) and fixed μ (T), as suggested from the fact that holes (plasminos) are more significant at higher temperatures [25]. In what follows, we will study the impact of this difference on the fermionic part of the shear viscosity.

2. Fermionic part of the shear viscosity

In Sec. III B, the fermionic part of the shear viscosity, η_f, was computed in terms of Γ_+ and Γ_- for vanishing chemical potential [see Eq. (3.49)]. In Appendix C, we present η_f for nonvanishing chemical potential [see Eq. (C1)]. Neglecting the contribution of $\mathfrak{Re}[\Sigma_R^f]$ in $E_\pm$ from Eq. (3.38) and in $\mathcal{E}_\pm$ from Eq. (C2), and replacing $E_\pm$ and $\mathcal{E}_\pm$, appearing in Eqs. (3.49) and (C1), with ω_f and $\omega_\pm = \omega_f \pm \mu$, respectively, we have plotted the T

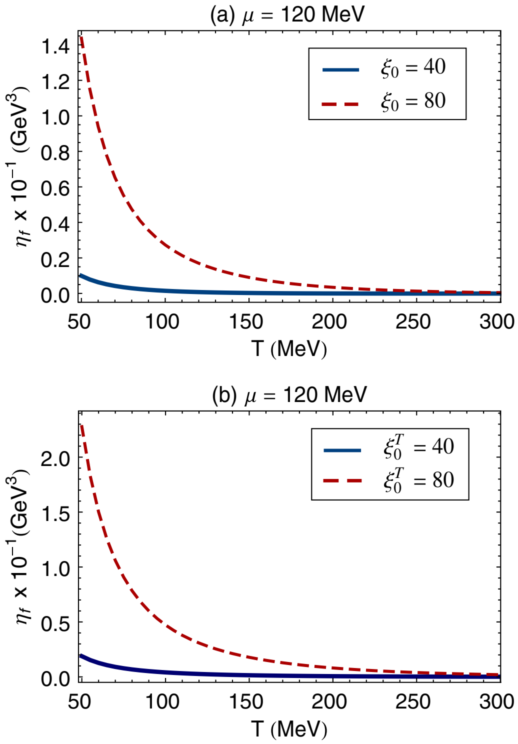

FIG. 16 (color online). The T dependence of η_f is plotted for $\mu = 120$ MeV and T-independent $\xi_0 = 40, 80$ arising from $m_b^0 = 200, 400$ MeV and $m_f^0 = 5$ MeV. (b) The T dependence of η_f, including the T- and μ-dependent thermal corrections to bosonic and fermionic masses, is plotted for $m_b^0 = 200, 400$ MeV and $m_f^0 = 5$ MeV, leading to $\xi_0^T = 40, 80$.

dependence of η_f for fixed $\mu = 120$ MeV and $\xi_0 = 40, 80$ in Fig. 16(a) and for $\mu = 120$ MeV and $\xi_0^T = 40, 80$ in Fig. 16(b). In contrast to the T dependence of η_b from Fig. 10, we observe that η_f decreases with increasing T, η_f is in general larger than η_b, and at a fixed temperature and for a fixed chemical potential, η_f increases with increasing ξ_0 [Fig. 16(a)] as well as ξ_0^T [Fig. 16(b)]. The fact that for a fixed T and μ, η_f decreases with increasing ξ_0 is compatible with the results arising from Fig. 12, where it is shown that $\Gamma_\pm$ increases with increasing ξ_0, and confirms the fact that for small values of ξ_0 (or ξ_0^T), $\eta_f \sim \Gamma_\pm^{-1}$. But, in general, it seems that the thermal property of η_f is dominated by the thermal behavior of Γ_-. The fact that η_f is inversely proportional to the fermionic spectral width coincides with the results presented in Ref. [30], and indicates that η_f increases with an increase in the mean free path.[1]

In Fig. 17, the μ dependence of η_f is plotted for $T = 120$ MeV and $\xi_0 = 40$ (blue solid line) and $\xi_0^T = 40$ (red dashed line). In contrast to the μ dependence of η_b from Fig. 11, η_f decreases with increasing μ at a fixed temperature. Moreover, at a fixed T and μ, η_f decreases when the

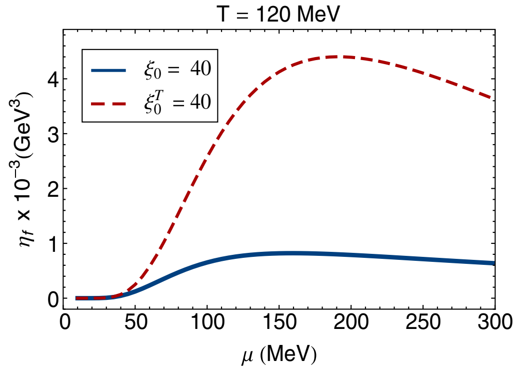

FIG. 17 (color online). The μ dependence of η_f is plotted for $T = 120$ MeV and $\xi_0 = \xi_0^T = 40$.

thermal corrections to the bosonic and fermionic masses are taken into account. This is again in contrast with the observed results for η_b in Fig. 11.

As we have shown in Figs. 13, 14 and 15, Γ_+ and Γ_- have different thermal properties. To study how this difference can affect η_f, we define a quantity Δ, as the difference between η_f as a functional of $\Gamma_+ = \Gamma_-$, and η_f as a functional of $\Gamma_+ \neq \Gamma_-$,

$$\Delta = \eta_f[\Gamma_+ = \Gamma_-] - \eta_f[\Gamma_+ \neq \Gamma_-]. \tag{5.4}$$

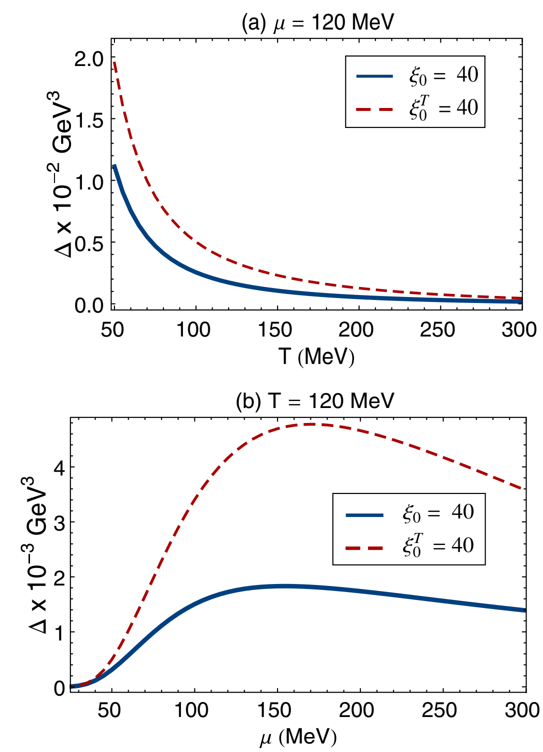

FIG. 18 (color online). (a) The T dependence of Δ, defined in Eq. (5.4), is plotted for $\mu = 120$ MeV and $\xi_0 = \xi_0^T = 40$. (b) The μ dependence of Δ is plotted for $T = 120$ MeV and $\xi_0 = \xi_0^T = 40$. As it turns out, Δ decreases (increases) with increasing T (μ) and constant-mass ratio ξ_0 as well as ξ_0^T.

[1] In Ref. [30], no difference was made between the mean free paths of normal and plasmino excitations.

Let us recall, that in the literature the difference between Γ_+ and Γ_- is often neglected, and so far, $\Delta \simeq 0$ has been assumed. In Figs. 18(a) and (b), the T and μ dependence of Δ is plotted for constant $\mu = 120$ MeV [panel (a)] and $T = 120$ MeV [panel (b)], and for $\xi_0 = 40$ (blue solid lines) and $\xi_0^T = 40$ (red dashed lines). It turns out that in the whole range of T and μ, Δ is positive. This means that the value of η_f increases, when the difference between Γ_+ and Γ_- is neglected. Moreover, for fixed μ (T) and constant ξ_0 or ξ_0^T, Δ decreases (increases) with T (μ). In other word, as it is shown in Fig. 18(a), whereas at lower temperatures and for an intermediate value of μ, the difference between $\eta_f[\Gamma_+ = \Gamma_-]$ and $\eta_f[\Gamma_+ \neq \Gamma_-]$ is relatively large, and becomes larger by including the thermal corrections to the bosonic and fermionic masses, it can be neglected at higher temperatures. In contrast, the difference between $\eta_f[\Gamma_+ = \Gamma_-]$ and $\eta_f[\Gamma_+ \neq \Gamma_-]$ is negligible at fixed temperatures and for small values of the chemical potential. It increases with increasing μ and is enhanced by adding the thermal corrections to the bosonic and fermionic masses.

VI. SUMMARY AND OUTLOOK

The shear viscosity η is a transport coefficient, that characterizes the diffusion of momentum transverse to the direction of propagation. It plays an important role in the physics of the QGP. In the past few years, there have been several attempts to explore its thermal properties, in particular in the vicinity of the QCD chiral transition point. The aim is to determine the position of the transition temperature of QCD, using the thermal properties of η, in addition to and independently of the equation of state [2]. In this paper, we studied the thermal properties of the shear viscosity of an interacting boson-fermion system with the Yukawa coupling. We followed the method presented in Ref. [18] to derive the bosonic part of the shear viscosity of this theory in terms of the bosonic spectral width, Γ_b. The latter was then determined in a one-loop perturbative expansion in orders of the Yukawa coupling. Using $\eta_b[\Gamma_b]$, it was then possible to study the thermal properties of η_b, in addition to its dependence on the masses of bosons and fermions.

We took the method used in Ref. [18], as our guideline, and determined the fermionic part of the shear viscosity of the Yukawa theory in terms of the fermionic widths Γ_+ and Γ_-. The expression $\eta_f[\Gamma_\pm]$ from Eqs. (3.49) and (C1) for vanishing and nonvanishing chemical potential, contains the central analytical results of the present paper. Here, Γ_+ and Γ_- are the spectral widths, corresponding to the normal and collective (plasmino) excitations of fermions. They were studied very intensively in the literature and led e.g. to structures in the low-mass dilepton production rate, which might provide a unique signature for the QGP formation in relativistic heavy-ion collisions [27]. However, to the best of our knowledge, the difference between their spectral widths is often neglected (see e.g. Refs. [17,23,33]), and, as in Refs. [19,29], the fermionic spectral density function, ρ_f, is given in terms of one and the same fermionic spectral width. We, however, used the structure of ρ_f presented in Ref. [30], including both Γ_+ and Γ_-, and following the method presented in Ref. [18], determined $\eta_f[\Gamma_\pm]$ in an appropriate Laurent expansion. Moreover, we completed the results presented in Ref. [30], and evaluated $\Gamma_\pm$ in a one-loop perturbative expansion in orders of the Yukawa coupling, and studied their thermal properties. Then, by plugging $\Gamma_\pm$ into the proposed relation for the fermionic shear viscosity, $\eta_f[\Gamma_\pm]$ from Eqs. (3.49) and (C1), we determined the thermal properties of η_f, and studied its mass dependence. Apart from various results on the thermal properties of $\Gamma_b, \Gamma_\pm$ as well as η_b and η_f, discussed in the previous section, we showed that, depending on the temperature and/or chemical potential, $\eta_f[\Gamma_+ \neq \Gamma_-]$ is smaller than $\eta_f[\Gamma_+ = \Gamma_-]$.

It shall be noted that our one-loop computation, including bare fermion and boson masses, is incomplete and can be improved, for instance, by considering the full HTL correction to the fermion propagator. The latter plays a crucial role in determining Γ_b and $\Gamma_\pm$, and consequently η_b and η_f. This drawback is partly compensated in the present paper by adding thermal corrections to the bosonic and fermionic masses. This *ad hoc* treatment of thermal masses seems to be natural, since, as was also discussed in Refs. [23,24], it equals the HTL treatment with an approximate fermion propagator. Moreover, since it is known that the HTL/hard-density-loop treatments are only valid for soft momenta $p \lesssim gT, g\mu$, even the HTL treatment can be improved by studying the ultra-soft fermionic excitations, with $p \lesssim g^2T, g^2\mu$. They were recently discussed in Refs. [34,35], in the framework of the Yukawa theory. An important question related to the perturbative treatment of transport coefficients, in general, and shear viscosity, in particular, is the appearance of the so-called pinch singularities, which would break the perturbation theory based on a loop expansion. A useful description of these singularities was presented in Ref. [16]: in the quasiparticle approximation, where the propagators are given by the energy and spectral widths of the quasiparticles, the pinch singularity is essentially related to the IR behavior of the product of retarded and advanced propagators, which appears in the perturbative loop calculations. Once the spectral width is zero, the above-mentioned product becomes IR divergent. The consequence is that higher-loop diagrams, if they are sufficiently IR sensitive, become as important as the one-loop contribution, and a resummation of an infinite number of ladder diagrams will be necessary. In Ref. [11], a detailed power counting was presented for $\lambda\varphi^3$ and $\lambda\varphi^4$ theories, and it was shown that all ladder diagrams contribute in the same leading order. In Ref. [34], a similar power counting was performed for the ladder diagrams contributing to the fermion self-energy of a Yukawa theory, and it was shown that in contrast to the above-mentioned scalar theories with cubic and quartic interactions, and also in sharp contrast to QED and QCD, the ladder diagrams are indeed suppressed, and consequently the one-loop self-energy diagram with dressed propagators (including the thermal masses) gives the leading-order contribution to the fermion self-energy. The main reason for this suppression is the fact that the Yukawa coupling constant receives no correction in the leading-order HTL approximation. Or, as was stated in Ref. [34], “the ladder diagrams giving a vertex correction do not contribute in the leading order in the scalar coupling”. As concerns higher-loop contributions to the spectral width and shear viscosity of the Yukawa theory, it seems therefore that no ladder resummation may be necessary, and the one-loop computation, including the thermal masses, may provide the leading-order contribution to these quantities. A recent perturbative computation of the shear viscosity of the Yukawa theory up to two-loop order confirmed this conclusion [40]. It was, in particular, shown that the two-loop diagrams, having the same power of coupling as the one-loop diagram, is substantially suppressed compared to one-loop contribution. According to the arguments presented in Ref. [40], it is indeed expected that by increasing the number of loops, the suppression successively grows, so that the one-loop results of the shear viscosity of the Yukawa-Fermi gas can be considered as the leading order. A more detailed analysis of ladder resummation corresponding to the shear viscosity of the Yukawa theory will be postponed to a future publication.

In Sec. IV, the leading-order contributions to the bosonic and fermionic spectral widths of the Yukawa theory were determined by computing the imaginary part of two one-loop bosonic and fermionic self-energy diagrams (see Figs. 3 and 4). Let us notice at this stage, that these one-loop contributions correspond to $1\to 2$ scattering processes (Landau damping), which seem to build the leading-order contribution to the spectral widths of the Yukawa theory. This is again in contrast to the situation appearing in QED, where, as was argued by Gagnon and Jeon in Ref. [29], apart from the special case of $1\to 2$ collinear scatterings including massless electrons, the perturbative series of the spectral widths starts from the leading $2\to 2$ scattering processes, arising from two-loop self-energies. This is because of the fact that in QED, in contrast to the Yukawa theory, the imaginary parts of the one-loop boson (photon) and fermion (electron) self-energies vanish, as can be easily checked, and as was also stated in Ref. [29]. Hence, an on-mass-shell massless excitation cannot decay into two on-mass-shell excitations, as expected. We can therefore conclude that in the Yukawa theory, the $2\to 2$ scattering processes, arising from two-loop contributions to the bosonic and fermionic self-energies provide the subleading contribution to the spectral widths of this theory relative to $1\to 2$ scattering processes, arising from the one-loop self-energy diagrams demonstrated in Figs. 3 and 4 of the present paper.

Let us finally notice that one of the possibilities to extend the present computation is to apply it to a QCD-like model, e.g. quark-meson or NJL models, including spontaneous or dynamical chiral symmetry breaking, and to study the behavior of η in the vicinity of the chiral transition point. The latter project is currently under investigation. The results will be reported elsewhere.

APPENDIX A: SPECTRAL DENSITY FUNCTION OF FERMIONS

In this appendix, we will apply the method presented in Ref. [28] for massive fermions, and will show that the spectral density function of fermions is given by Eq. (3.36). To start, let us consider the Källen-Lehmann representation of a free fermion propagator in terms of the free spectral density function ρ_f^0,

$$S_0(\mathbf{p},\omega)=\int_{-\infty}^{+\infty}\frac{dp_0}{2\pi}\frac{\rho_f^0(\mathbf{p},p_0)}{p_0-\omega}. \tag{A1}$$

Plugging

$$\rho_f^0(\mathbf{p},p_0)=2\pi(p\cdot\gamma+m_f)\mathrm{sgn}(p_0)\delta(p_0^2-\omega_f^2), \tag{A2}$$

with $\omega_f^2=\mathbf{p}^2+m_f^2$, into Eq. (A1), and integrating over p_0, we arrive at the following decomposition of S_0 in terms of two independent matrices $\hat{g}_\pm$, defined in Eq. (3.37):

$$S_0(\mathbf{p},\omega)=-\frac{1}{\omega-\omega_f}\hat{g}_+-\frac{1}{\omega+\omega_f}\hat{g}_-. \tag{A3}$$

To determine the inverse propagator of free fermions, we introduce the new matrices

$$\hat{g}'_\pm\equiv\frac{1}{2\omega_f}[\gamma_0\omega_f\mp(\gamma.\mathbf{p}+m_f)] \tag{A4}$$

that satisfy

$$\begin{aligned}(\hat{g}'_\pm)^\dagger&=\hat{g}_\mp, & \hat{g}_\pm\hat{g}'_\pm&=0,\\ \hat{g}'_\mp\hat{g}_\pm&=\hat{g}'_\mp\gamma_0, & \hat{g}_\pm\hat{g}'_\mp&=\gamma_0\hat{g}'_\mp.\end{aligned} \tag{A5}$$

The inverse propagator of free fermions is then given by

$$S_0^{-1}(\mathbf{p},\omega)=-(\omega+\omega_f)\hat{g}'_+-(\omega-\omega_f)\hat{g}'_-. \tag{A6}$$

To determine the dressed spectral density $\rho_f(\omega,p_0)$ for the dressed fermion propagator $S(\mathbf{p},\omega)$, let us now consider the inverse fermion propagator,

$$S^{-1}(\mathbf{p},\omega)=S_0^{-1}(\mathbf{p},\omega)+\Sigma^f(\mathbf{p},\omega), \tag{A7}$$

where $\Sigma(\mathbf{p},\omega)$ is the fermion self-energy, including all one-particle-irreducible radiative corrections, corresponding to the two-point Green's function of fermions. By decomposing Σ^f as

$$\Sigma^f(\mathbf{p},\omega) = \hat{g}'_-\Sigma_+(\omega,\mathbf{p}) - \hat{g}'_+\Sigma_-(\omega,\mathbf{p}), \tag{A8}$$

and combining the resulting expression with Eq. (A6), we arrive, according to Eq. (A7), at

$$S^{-1}(\mathbf{p},\omega) = -\hat{g}'_+(\omega+\omega_f+\Sigma_-) - \hat{g}'_-(\omega-\omega_f-\Sigma_+). \tag{A9}$$

Using the identities (A5) for $\hat{g}_\pm$ and $\hat{g}'_\pm$, it is easy to show that $\Sigma_\pm$ from Eq. (A8) is given by

$$\Sigma_\pm = \pm\frac{1}{2}\mathrm{tr}(\hat{g}_\pm\Sigma^f). \tag{A10}$$

By inverting Eq. (A9), and by making use of the properties (A5), the dressed fermion propagator reads

$$S(\mathbf{p},\omega) = -\frac{1}{\omega-(\omega_f+\Sigma_+)}\hat{g}_+ - \frac{1}{\omega+(\omega_f+\Sigma_-)}\hat{g}_-. \tag{A11}$$

Using at this stage the definition $\rho_f = -2\mathfrak{Im}[S_R]$, and introducing

$$E_\pm \equiv \omega_f + \mathfrak{Re}[\Sigma_\pm^R], \tag{A12}$$

as well as

$$\Gamma_\pm \equiv \mathfrak{Im}[\Sigma_\pm^R], \tag{A13}$$

we arrive at $\rho_f(\mathbf{p},\omega)$ from Eq. (3.36). Let us finally notice that $E_\pm$ and $\Gamma_\pm$ defined in Eq. (3.38), arise by plugging Eq. (A10) into Eqs. (A12) and (A13) and neglecting the imaginary part of $\hat{g}_\pm$, defined in Eq. (3.37).

APPENDIX B: COMPUTATION OF EQS. (4.14) AND (4.19)

In this appendix, we will perform analytically the three-dimensional k-integration in Eqs. (4.13) and (4.18) to arrive at Eqs. (4.14) and (4.19), respectively. We also present the final result for Γ_f^-.

Let us start by considering the integral

$$\mathcal{I} = \int\frac{d^3k}{(2\pi)^2 2\omega_1 2\omega_2}\delta(\omega_b-\omega_1-\omega_2)f(\omega_b,\omega_1,\omega_2), \tag{B1}$$

where $f(\omega_b,\omega_1,\omega_2)$ is a generic function of ω_i, $i=b,1,2$. According to the definitions in Sec. IVA, $\omega_b^2 = \mathbf{p}^2+m_b^2$, $\omega_1^2 = \mathbf{k}^2+m_f^2$ and $\omega_2^2 = (\mathbf{k}-\mathbf{p})^2+m_f^2$. Denoting the angle between $\mathbf{k}$ and $\mathbf{p}$ by θ_p, and inserting

$$1 = \frac{1}{2}\int d(\cos\theta_p) \tag{B2}$$

into the integration over k, appearing in Eq. (B1), we arrive at

$$\begin{aligned}\mathcal{I} &= \frac{1}{2}\int\frac{d^3k}{(2\pi)^2 2\omega_1}\frac{d(\cos\theta_p)}{2\omega_2}\\ &\quad\times\delta(\omega_b-\omega_1-\omega_2)f(\omega_b,\omega_1,\omega_2)\\ &= \frac{1}{2}\int\frac{d^3k}{(2\pi)^2 2\omega_1}\int d\omega_2\left(\frac{d\omega_2^2}{d(\cos\theta_p)}\right)^{-1}\\ &\quad\times\delta(\omega_b-\omega_1-\omega_2)f(\omega_b,\omega_1,\omega_2)\\ &= -\frac{1}{8\pi|\mathbf{p}|}\int d\omega_1 f(\omega_b,\omega_1,\omega_2=\omega_b-\omega_1).\end{aligned} \tag{B3}$$

To derive the above relation, the identity

$$\omega_2^2 = \omega_1^2+\mathbf{p}^2-2|\mathbf{p}||\mathbf{k}|\cos\theta_p \tag{B4}$$

arising from the definition of ω_2 in terms of $\mathbf{p}$ and $\mathbf{k}$ is used. The latter identity can also be used to determine the range of integration over ω_1 in Eq. (B3). Having in mind that

$$-1 \le \cos\theta_p = \frac{\omega_1^2+\mathbf{p}^2-\omega_2^2}{2|\mathbf{k}||\mathbf{p}|} \le +1, \tag{B5}$$

we arrive at

$$\omega_1^2 - \omega_1\omega_b + \frac{m_b^4+4m_f^2\mathbf{p}^2}{4m_b^2} \le 0, \tag{B6}$$

whose solution yields $\alpha_b^- \le \omega_1 \le \alpha_b^+$, with

$$\alpha_b^\pm \equiv \frac{1}{2}\left(\omega_b \pm \frac{|\mathbf{p}|}{\xi}\sqrt{\xi^2-4}\right), \tag{B7}$$

and $\xi = \frac{m_b}{m_f}$. Plugging

$$f(\omega_b,\omega_1,\omega_2) = \frac{g^2(4m_f^2-m_b^2)}{4\omega_b}\frac{\sinh(\frac{\beta\omega_b}{2})}{\cosh(\frac{\beta\omega_1}{2})\cosh(\frac{\beta\omega_2}{2})} \tag{B8}$$

from Eq. (4.13) into the expression on the rhs of Eq. (B3), we arrive after some straightforward manipulations at Eq. (4.14).

To derive Eq. (4.19), let us now consider Eq. (4.18), where in contrast to the previous case two δ functions $\delta(\omega_f\mp\omega_1\pm\omega_2)$ contribute to Γ_+. Having in mind that in the fermionic case $\omega_f^2 = \mathbf{p}^2+m_f^2$, $\omega_1^2 = \mathbf{k}^2+m_f^2$ and $\omega_2^2 = (\mathbf{k}-\mathbf{p})^2+m_b^2$, we obtain $\omega_2^2 = \omega_1^2+\mathbf{p}^2-2|\mathbf{p}||\mathbf{k}|\cos\theta_p+m_b^2-m_f^2$. Following now the same steps leading from Eq. (B1) to Eq. (B3), we arrive at

$$\int \frac{d^3k}{(2\pi)^2 2\omega_1 2\omega_2}\delta(\omega_f \mp \omega_1 \pm \omega_2) f(\omega_f,\omega_1,\omega_2) = -\frac{1}{8\pi|\mathbf{p}|}\int d\omega_1 f(\omega_f,\omega_1,\omega_2=\omega_1\mp\omega_f). \tag{B9}$$

As concerns the range of integration over ω_1, we can use

$$-1 \le \cos\theta_p = \frac{\omega_1^2-\omega_2^2+\mathbf{p}^2+m_b^2-m_f^2}{2|\mathbf{k}||\mathbf{p}|} \le +1$$

to get

$$\omega_1^2 \pm (\xi^2-2)\omega_f\omega_1 + \mathbf{p}^2 + \frac{m_f^2}{4}(\xi^2-2)^2 \le 0. \tag{B10}$$

Here, the $\pm$ signs before the second term correspond to $\omega_2=\omega_1\mp\omega_f$, respectively. Solving the above equation, we arrive for $\omega_2=\omega_1-\omega_f$ at $m_f\le\omega_1\le\alpha_f^+$, with

$$\alpha_f^+ \equiv \frac{-\omega_f(\xi^2-2)+|\mathbf{p}|\xi\sqrt{\xi^2-4}}{2}, \tag{B11}$$

and for $\omega_2=\omega_1+\omega_f$ at $\beta_f^-\le\omega_1\le\beta_f^+$, with

$$\beta_f^\pm \equiv \frac{\omega_f(\xi^2-2)\pm|\mathbf{p}|\xi\sqrt{\xi^2-4}}{2}. \tag{B12}$$

Plugging Eqs. (B11) and (B12) into Eq. (B9), and using the resulting expression, the three-dimensional k integration in Eq. (4.18) can be performed analytically. We arrive after some algebra at Eq. (4.19).

To evaluate Γ_f^- from Eq. (4.18), we follow the same procedure as above. Using

$$\int \frac{d^3k}{(2\pi)^2 2\omega_2}[\delta(\omega_f-\omega_1+\omega_2)+\delta(\omega_f+\omega_1-\omega_2)] f(\omega_f,\omega_1,\omega_2) = -\frac{1}{4\pi|\mathbf{p}|}\left[\int_{m_f}^{\alpha_f^+} d\omega_1\omega_1 f(\omega_f,\omega_1,\omega_2=\omega_1-\omega_f) + \int_{\beta_f^-}^{\beta_f^+} d\omega_1\omega_1 f(\omega_f,\omega_1,\omega_2=\omega_1+\omega_f)\right], \tag{B13}$$

with

$$f(\omega_f,\omega_1,\omega_2) = \frac{g^2}{4}\frac{\cosh(\frac{\beta\omega_f}{2})}{\cosh(\frac{\beta\omega_1}{2})\sinh(\frac{\beta\omega_2}{2})},$$

and

$$\int du u(\coth u)^{\pm 1} = \frac{1}{2}[u(u+2\ln(1\mp e^{-2u})) - \mathrm{Li}_2(\pm e^{-2u})],$$

we arrive at

$$\Gamma_f^- = -\frac{g^2T}{8\pi\kappa_f\sqrt{1-\gamma_f^2}}\left\{\kappa_f\ln\left[\frac{1-\cosh(2\Xi_-)}{\cosh(\Upsilon_-+\Xi_+)-\cosh(\Upsilon_--\Xi_+)}\right] + [u(u+2\ln(1-e^{-2u}))-\mathrm{Li}_2(e^{-2u})]|_{\Upsilon_-}^{-\Xi_-} + [u(u+2\ln(1-e^{-2u}))-\mathrm{Li}_2(e^{-2u})]|_{\Xi_-}^{\Xi_+} - [u(u+2\ln(1+e^{-2u}))-\mathrm{Li}_2(-e^{-2u})]|_{\Upsilon_-+\frac{\kappa_f}{2}}^{-\Xi_-+\frac{\kappa_f}{2}} - [u(u+2\ln(1+e^{-2u}))-\mathrm{Li}_2(-e^{-2u})]|_{\Xi_--\frac{\kappa_f}{2}}^{\Xi_+-\frac{\kappa_f}{2}}\right\}, \tag{B14}$$

where κ_f, $\Xi_\pm$ and $\Upsilon_\pm$ are defined below Eq. (4.19) and in Eq. (4.20).

APPENDIX C: SHEAR VISCOSITY AND SPECTRAL WIDTH OF FERMIONS FOR NONVANISHING CHEMICAL POTENTIAL

In this appendix, we will first determine the fermionic spectral widths $\Gamma_\pm$ and shear viscosity η_f for nonvanishing chemical potential. To do this, we will follow the method described in Sec. III B and Appendix A. We will then use the method presented in Sec. IV and Appendix B, and derive the one-loop contribution to the bosonic and fermionic spectral widths for nonvanishing temperature and chemical potential.

1. Fermionic contribution to η_f for $\mu \neq 0$

In what follows, we will show that in the one-loop skeleton expansion, the fermionic part of the shear viscosity η_f, is given by

$$\eta_f \sim \frac{2\beta}{15\pi^2}\int_0^\infty dp\,\frac{\mathbf{p}^4}{\omega_f^2}\sum_{s=\pm}\left\{\frac{e^{\beta(\mathcal{E}_s - s\mu)}}{(e^{\beta(\mathcal{E}_s-s\mu)}+1)^2}\times\left[\frac{\mathbf{p}^2}{\Gamma_s} - \frac{4m_f^2(\Gamma_f^+ - \Gamma_s)}{[\mathcal{E}_f + is\Gamma_f^+][\mathcal{E}_f + i\Gamma_f^-]}\right]\right\}, \tag{C1}$$

where $\mathcal{E}_f = \mathcal{E}_+ + \mathcal{E}_-$ and $\Gamma_f^\pm = \Gamma_+ \pm \Gamma_-$, similar to the definitions in Eq. (3.48). Here, in contrast to $E_\pm$ defined in Eq. (3.38), the $\mathcal{E}_\pm$ appearing in $\mathcal{E}_f$ are given by

$$\mathcal{E}_\pm(\mathbf{p},\omega_\pm) \equiv \omega_\pm \pm \frac{1}{2}\mathrm{tr}(\hat{g}_\pm(\mathbf{p},\omega_f)\mathfrak{Re}[\Sigma_R^f(\mathbf{p},\omega_f)]), \tag{C2}$$

where $\omega_\pm \equiv \omega_f \pm \mu$. To derive Eq. (C1), we start, as in Appendix A, with the Källen-Lehmann representation of the free fermion propagator in terms of the free spectral density function, ρ_f^0,

$$S_0(\mathbf{p},\omega) = \int_{-\infty}^\infty \frac{dp_0}{2\pi}\frac{\rho_f^0(\mathbf{p},p_0)}{p_0+\mu-\omega}, \tag{C3}$$

where $\rho_f^0(\mathbf{p},p_0)$ is defined in Eq. (A2). Integrating over p_0, we arrive at a decomposition, similar to what is demonstrated in Eq. (A3),

$$S_0(\mathbf{p},\omega) = -\frac{1}{\omega-\omega_+}\hat{g}_+ - \frac{1}{\omega+\omega_-}\hat{g}_-. \tag{C4}$$

Here, $\omega_\pm = \omega_f \pm \mu$ and $\hat{g}_\pm$ are defined in Eq. (3.37). Following now the same steps as described in Appendix A, we arrive first at the dressed fermion propagator for nonvanishing μ,

$$S(\mathbf{p},\omega) = -\frac{1}{\omega-(\omega_+ + \Sigma_+)}\hat{g}_+ - \frac{1}{\omega+(\omega_-+\Sigma_-)}\hat{g}_-, \tag{C5}$$

where $\Sigma_\pm$ are given in Eq. (A10). Using at this stage $\rho_f = -2\mathfrak{Im}[S_R]$, we arrive at

$$\rho_f(\mathbf{p},\omega) = \frac{2\Gamma_+(\mathbf{p},\omega_f)}{[\omega-\mathcal{E}_+(\mathbf{p},\omega_f]^2+\Gamma_+^2(\mathbf{p},\omega_f)}\hat{g}_+(\mathbf{p},\omega_f) - \frac{2\Gamma_-(\mathbf{p},\omega_f)}{[\omega+\mathcal{E}_-(\mathbf{p},\omega_f)]^2+\Gamma_-^2(\mathbf{p},\omega_f)}\hat{g}_-(\mathbf{p},\omega_f), \tag{C6}$$

with $\mathcal{E}_\pm$ defined in Eq. (B2) and $\Gamma_\pm$ in Eq. (3.38). Then, by plugging the standard representation

$$S_T(\mathbf{p},\omega_n) = \frac{1}{2\pi}\int_{-\infty}^{+\infty} d\omega\,\frac{\rho_f(\mathbf{p},\omega)}{i\omega_n-\omega+\mu} \tag{C7}$$

into Eq. (3.29) and performing the summation over Matsubara frequencies ω_n, we arrive at

$$S_T(\mathbf{p},\tau) = \frac{1}{2\pi}\int_{-\infty}^{+\infty} d\omega e^{(\mu-\omega)\tau}\rho_f(\mathbf{p},\omega)\times(\theta(-\tau)n_f^+(\omega) - \theta(\tau)(1-n_f^+(\omega))), \tag{C8}$$

which replaces Eq. (3.30). Here, fermionic distribution functions, including μ, are defined by

$$n_f^\pm(\omega) \equiv \frac{1}{e^{\beta(\omega\mp\mu)}+1}. \tag{C9}$$

Plugging now $S_T(\mathbf{p},\tau)$ from Eq. (C8) into Eq. (3.9), and following the same steps leading from Eq. (3.33) to Eq. (3.49), we arrive at $\eta_f[\Gamma_\pm]$ from Eq. (C1).

2. Bosonic and fermionic spectral widths for $\mu \neq 0$

To determine the one-loop contributions to Γ_b and $\Gamma_\pm$ for nonvanishing chemical potential, we will follow the method described in Sec. IV, and will compute the imaginary part of the one-loop bosonic and fermionic self-energy diagrams, using the Schwinger-Keldysh real-time formalism [36]. Since the chemical potential is only introduced for fermions, the free propagator of scalar bosons remains unchanged [see Eqs. (4.1) and (4.2)]. As concerns the free fermion propagator, it is given for nonvanishing μ by

$$\mathcal{S} = \begin{pmatrix} S_{++} & S_{+-} \\ S_{-+} & S_{--}\end{pmatrix}, \tag{C10}$$

with $S_{ab}, a, b = \pm$ slightly different from Eq. (4.4),

$$\begin{aligned}
S_{++}(p) &= (\gamma\cdot p + m_f)\left(-\frac{i}{p^2-m_f^2+i\epsilon} + 2\pi\delta(p^2-m_f^2)[\theta(p_0)n_f(x_p)+\theta(-p_0)n_f(-x_p)]\right),\\
S_{+-}(p) &= -2\pi(\gamma\cdot p + m_f)[\theta(-p_0)(1-n_f(-x_p)) - \theta(p_0)n_f(x_p)],\\
S_{-+}(p) &= -2\pi(\gamma\cdot p + m_f)[\theta(p_0)(1-n_f(x_p)) - \theta(-p_0)n_f(-x_p)],\\
S_{--}(p) &= (\gamma\cdot p + m_f)\left(\frac{i}{p^2-m_f^2-i\epsilon} + 2\pi\delta(p^2-m_f^2)[\theta(p_0)n_f(x_p)+\theta(-p_0)n_f(-x_p)]\right),
\end{aligned} \tag{C11}$$

where x_p is defined by $x_p \equiv p_0 + \mu$ and $n_f(\omega)$ is given in Eq. (3.31). According to Eq. (4.9), the bosonic spectral width, Γ_b, is given by the imaginary part of Σ_R^b. At the one-loop level, $\mathfrak{Im}[\Sigma_R^b(p)]$ is given in Eq. (4.10). Using $S_{ab}, a, b = \pm$ from Eq. (C11), we arrive at

$$\Gamma_b(\mathbf{p},\omega_b) = \frac{g^2}{8\omega_b}\int \frac{d^3k}{(2\pi)^2}\frac{(4m_f^2-m_b^2)}{\omega_1\omega_2}\{\delta(\omega_b-\omega_1-\omega_2)[1-n_f^-(\omega_1)-n_f^+(\omega_2)] + \delta(\omega_b-\omega_1+\omega_2)[n_f^-(\omega_1)-n_f^-(\omega_2)] - \delta(\omega_b+\omega_1-\omega_2)[n_f^+(\omega_1)-n_f^+(\omega_2)] - \delta(\omega_b+\omega_1+\omega_2)[1-n_f^+(\omega_1)-n_f^-(\omega_2)]\}. \tag{C12}$$

Here, $n_f^\pm$ are defined in Eq. (C9). Following the same steps leading from Eq. (4.11) to Eq. (4.13), we first arrive after some work at

$$\Gamma_b(\mathbf{p},\omega_b) = \frac{g^2(4m_f^2-m_b^2)}{16\omega_b}\int \frac{d^3k}{(2\pi)^2}\frac{\sinh(\frac{\beta\omega_b}{2})}{\cosh(\frac{\beta(\omega_1+\mu)}{2})\cosh(\frac{\beta(\omega_2-\mu)}{2})}\frac{\delta(\omega_b-\omega_1-\omega_2)}{\omega_1\omega_2}, \tag{C13}$$

and finally, after performing the integration over k, using the method demonstrated in Appendix B, at

$$\Gamma_b(\mathbf{p},\omega_b) = \frac{g^2T}{16\pi}\frac{\gamma_b^2(\xi^2-4)}{\xi^2\sqrt{1-\gamma_b^2}}\ln\left[\frac{\cosh(\tau_f)+\cosh\frac{\kappa_b}{2}\left(1+\frac{1}{\xi}\sqrt{(\xi^2-4)(1-\gamma_b^2)}\right)}{\cosh(\tau_f)+\cosh\frac{\kappa_b}{2}\left(1-\frac{1}{\xi}\sqrt{(\xi^2-4)(1-\gamma_b^2)}\right)}\right], \tag{C14}$$

where apart from ξ, κ_b, γ_b which are defined below Eq. (4.14), $\tau_f \equiv \mu/T$.

As concerns the one-loop contribution to the fermionic spectral widths $\Gamma_\pm$ from Eq. (3.38), let us consider $\mathfrak{Im}[\Sigma_R^f]$ from Eq. (4.15). Using G_{ab} and S_{ab}, $a, b = \pm$ from Eqs. (4.2) and (B11), we arrive first at

$$\Gamma_\pm(\mathbf{p},\omega_f) = \pm\frac{g^2}{8\omega_f}\int \frac{d^3k}{(2\pi)^2}\frac{1}{\omega_1\omega_2}[[\omega_f\omega_1 \mp \mathbf{p}\cdot\mathbf{k} \pm m_f^2]\{\delta(\omega_f-\omega_1-\omega_2)[1-n_f^-(\omega_1)+n_b(\omega_2)] + \delta(\omega_f-\omega_1+\omega_2)[n_f^-(\omega_1)+n_b(\omega_2)]\} + [\omega_f\omega_1 \pm \mathbf{p}\cdot\mathbf{k} \mp m_f^2]\{\delta(\omega_f+\omega_1+\omega_2)[1-n_f^+(\omega_1) + n_b(\omega_2)] + \delta(\omega_f+\omega_1-\omega_2)[n_f^+(\omega_1)+n_b(\omega_2)]\}], \tag{C15}$$

with $n_f^\mp(\omega)$ and $n_b(\omega)$ defined in Eqs. (B9) and (3.15), respectively. Following the arguments described in Sec. IV B, the relevant expression of Γ_+ for nonvanishing μ is given by

$$\Gamma_+(\mathbf{p},\omega_f) = \frac{g^2}{32\omega_f}\int \frac{d^3k}{(2\pi)^2}\frac{(4m_f^2-m_b^2)}{\omega_1\omega_2}\frac{\cosh(\frac{\beta(\omega_f+\mu)}{2})}{\sinh(\frac{\beta\omega_2}{2})}\times\left\{\frac{\delta(\omega_f-\omega_1+\omega_2)}{\cosh(\frac{\beta(\omega_1+\mu)}{2})} - \frac{\delta(\omega_f+\omega_1-\omega_2)}{\cosh(\frac{\beta(\omega_1-\mu)}{2})}\right\}. \tag{C16}$$

Performing the three-dimensional integration over k, using the method described in Appendix B, we finally arrive at Γ_+ in terms of the dimensionless variables ξ, γ_f, κ_f and τ_f, defined in Sec. IV B,

$$\Gamma_+(\xi,\gamma_f,\kappa_f,\tau_f;T) = \frac{g^2T}{32\pi}\frac{\gamma_f^2(\xi^2-4)}{\sqrt{1-\gamma_f^2}}\left\{\ln\left[\frac{1-\cosh(2\Xi_-)}{\cosh(\Upsilon_-+\Xi_+)-\cosh(\Upsilon_--\Xi_+)}\right] - \ln\left[\frac{1+\cosh(2\Xi_- - (\kappa_f+\tau_f))}{\cosh(\Upsilon_-+\Xi_+)+\cosh(\Upsilon_+-\Xi_++\tau_f)}\right]\right\}. \tag{C17}$$

Here, $\Xi_\pm$ and $\Upsilon_\pm$ are defined in Eq. (4.20). The difference between Γ_+ and Γ_- is, according to Eq. (3.48), defined by $\Gamma_f^- = \Gamma_+ - \Gamma_-$. For nonvanishing μ, Γ_f^- is first given by

$$\Gamma_f^-(\mathbf{p},\omega_f) = \frac{g^2}{8}\int \frac{d^3k}{(2\pi)^2\omega_2}\frac{\cosh(\frac{\beta(\omega_f+\mu)}{2})}{\sinh(\frac{\beta\omega_2}{2})}\times\left\{\frac{\delta(\omega_f-\omega_1+\omega_2)}{\cosh(\frac{\beta(\omega_1+\mu)}{2})} + \frac{\delta(\omega_f+\omega_1-\omega_2)}{\cosh(\frac{\beta(\omega_1-\mu)}{2})}\right\}, \tag{C18}$$

and, after integrating over the three-momentum k, using the method described in Appendix B, it reads

$$\Gamma_f^- = -\frac{g^2 T}{8\pi\kappa_f\sqrt{1-\gamma_f^2}}\left\{\kappa_f \ln\left[\frac{1-\cosh(2\Xi_-)}{\cosh(\Upsilon_- + \Xi_+) - \cosh(\Upsilon_- - \Xi_+)}\right] + \tau_f \ln\left[\frac{1+\cosh(2\Xi_- - (\kappa_f+\tau_f))}{\cosh(\Upsilon_- + \Xi_+) + \cosh(\Upsilon_+ - \Xi_+ + \tau_f)}\right]\right.$$
$$+ [u(u + 2\ln(1-e^{-2u})) - \mathrm{Li}_2(e^{-2u})]\Big|_{\Upsilon_-}^{-\Xi_-} + [u(u + 2\ln(1-e^{-2u})) - \mathrm{Li}_2(e^{-2u})]\Big|_{\Xi_-}^{\Xi_+}$$
$$\left. - [u(u + 2\ln(1+e^{-2u})) - \mathrm{Li}_2(-e^{-2u})]\Big|_{\Upsilon_- + \frac{(\kappa_f+\tau_f)}{2}}^{-\Xi_- + \frac{(\kappa_f+\tau_f)}{2}} - [u(u + 2\ln(1+e^{-2u})) - \mathrm{Li}_2(-e^{-2u})]\Big|_{\Xi_- - \frac{(\kappa_f+\tau_f)}{2}}^{\Xi_+ - \frac{(\kappa_f+\tau_f)}{2}}\right\}. \quad \text{(C19)}$$

[1] I. Arsene *et al.* (BRAHMS Collaboration), Nucl. Phys. **A757**, 1 (2005); K. Adcox *et al.* (PHENIX Collaboration), Nucl. Phys. **A757**, 184 (2005); B. B. Back *et al.* (PHOBOS Collaboration), Nucl. Phys. **A757**, 28 (2005); J. Adams *et al.* (STAR Collaboration), Nucl. Phys. **A757**, 102 (2005); K. Aamodt *et al.* (ALICE Collaboration), Phys. Rev. Lett. **105**, 252302 (2010); D. Caffarri (ALICE Collaboration), Nucl. Phys. **A904–905**, 643 (2013).

[2] J. I. Kapusta, in *Relativistic Nuclear Collisions*, edited by R. Stock (Springer-Verlag, Berlin/Heidelberg, 2010).

[3] M. Luzum and J.-Y. Ollitrault, Nucl. Phys. **A904–905**, 377 (2013).

[4] P. Huovinen, P. F. Kolb, U. W. Heinz, P. V. Ruuskanen, and S. A. Voloshin, Phys. Lett. B **503**, 58 (2001); H.-J. Drescher, A. Dumitru, C. Gombeaud, and J.-Y. Ollitrault, Phys. Rev. C **76**, 024905 (2007); L. P. Csernai, J. I. Kapusta, and L. D. McLerran, Phys. Rev. Lett. **97**, 152303 (2006).

[5] P. Romatschke and U. Romatschke, Phys. Rev. Lett. **99**, 172301 (2007); P. Huovinen and D. Molnar, Phys. Rev. C **79**, 014906 (2009).

[6] H. Song, Nucl. Phys. **A904–905**, 114 (2013).

[7] P. B. Arnold, G. D. Moore, and L. G. Yaffe, J. High Energy Phys. 11 (2000) 001; P. B. Arnold, G. D. Moore, and L. G. Yaffe, J. High Energy Phys. 05 (2003) 051; 01 (2003) 030; A. S. Khvorostukhin, V. D. Toneev, and D. N. Voskresensky, Phys. Rev. C **83**, 035204 (2011); S. Plumari, A. Puglisi, F. Scardina, and V. Greco, Phys. Rev. C **86**, 054902 (2012); S. Plumari, A. Puglisi, M. Colonna, F. Scardina, and V. Greco, J. Phys. Conf. Ser. **420**, 012029 (2013); S. Mattiello, arXiv:1210.1038; S. Mitra and S. Sarkar, Phys. Rev. D **87**, 094026 (2013).

[8] C. Sasaki and K. Redlich, Nucl. Phys. **A832**, 62 (2010).

[9] S. Ghosh, A. Lahiri, S. Majumder, R. Ray, and S. K. Ghosh, Phys. Rev. C **88**, 068201 (2013).

[10] D. N. Zubarev, *Nonequilibrium statistical thermodynamics* (Plenum, New York, 1974).

[11] S. Jeon, Phys. Rev. D **52**, 3591 (1995).

[12] P. F. Kelly, Q. Liu, C. Lucchesi, and C. Manuel, Phys. Rev. D **50**, 4209 (1994); D. F. Litim and C. Manuel, Nucl. Phys. **B562**, 237 (1999); E. Wang and U. W. Heinz, Phys. Lett. B **471**, 208 (1999); Phys. Rev. D **67**, 025022 (2003); V. Ozvenchuk, O. Linnyk, M. I. Gorenstein, E. L. Bratkovskaya, and W. Cassing, Phys. Rev. C **87**, 064903 (2013).

[13] G. Aarts and J. M. Martinez Resco, Nucl. Phys. B, Proc. Suppl. **119**, 505 (2003); A. Amato, G. Aarts, C. Allton, P. Giudice, S. Hands, and J.-I. Skullerud, arXiv:1310.7466.

[14] G. Aarts, D. Ahrensmeier, R. Baier, J. Berges, and J. Serreau, Phys. Rev. D **66**, 045008 (2002); G. Aarts and J. M. Martinez Resco, Phys. Rev. D **68**, 085009 (2003); M. E. Carrington, Acta Phys. Pol. B Proc. Suppl. **5**, 659 (2012); M. E. Carrington and E. Kovalchuk, Phys. Rev. D **81**, 065017 (2010).

[15] P. Kovtun, D. T. Son, and A. O. Starinets, Phys. Rev. Lett. **94**, 111601 (2005).

[16] Y. Hidaka and T. Kunihiro, Phys. Rev. D **83**, 076004 (2011).

[17] W. M. Alberico, S. Chiacchiera, H. Hansen, A. Molinari, and M. Nardi, Eur. Phys. J. A **38**, 97 (2008); P. Czerski, W. M. Alberico, S. Chiacchiera, A. De Pace, H. Hansen, A. M Olinari, and M. Nardi, J. Phys. G **36**, 025008 (2009).

[18] R. Lang, N. Kaiser, and W. Weise, Eur. Phys. J. A **48**, 109 (2012).

[19] R. Lang and W. Weise, Eur. Phys. J. A **50**, 63 (2014).

[20] S.-i. Nam and C.-W. Kao, Phys. Rev. D **87**, 114003 (2013).

[21] Y. Nambu and G. Jona-Lasinio, Phys. Rev. **122**, 345 (1961); **124**, 246 (1961); S. P. Klevansky, Rev. Mod. Phys. **64**, 649 (1992); M. Buballa, Phys. Rep. **407**, 205 (2005).

[22] M. Iwasaki, H. Ohnishi, and T. Fukutome, arXiv:hep-ph/0606192.

[23] C. P. Kiessig, M. Plumacher, and M. H. Thoma, Phys. Rev. D **82**, 036007 (2010).

[24] C. P. Kiessig and M. Plumacher, AIP Conf. Proc. **1200**, 999 (2010).

[25] H. A. Weldon, Phys. Rev. D **40**, 2410 (1989).

[26] H. A. Weldon, Phys. Rev. D **61**, 036003 (2000).

[27] E. Braaten, R. D. Pisarski, and T.-C. Yuan, Phys. Rev. Lett. **64**, 2242 (1990); E. Braaten and R. D. Pisarski, Phys. Rev. D **46**, 1829 (1992); J. I. Kapusta, P. Lichard, and D. Seibert, Phys. Rev. D **44**, 2774 (1991); **47**, 4171(E) (1993); A. Peshier and M. H. Thoma, Phys. Rev. Lett. **84**, 841 (2000).

[28] J.-P. Blaizot and E. Iancu, Phys. Rev. D **55**, 973 (1997).

[29] M. A. Valle Basagoiti, Phys. Rev. D **66**, 045005 (2002); J.-S. Gagnon and S. Jeon, Phys. Rev. D **76**, 105019 (2007).
[30] M. Iwasaki, H. Ohnishi, and T. Fukutome, J. Phys. G **35**, 035003 (2008); T. Fukutome and M. Iwasaki, Prog. Theor. Phys. **119**, 991 (2008).
[31] H. Liu, D. Hou, and L. Jiarong, arXiv:hep-ph/0602221; H. Liu, D.-F. Hou, and J.-R. Li, Commun. Theor. Phys. **50**, 429 (2008).
[32] D. Satow, Phys. Rev. D **87**, 096011 (2013).
[33] M. H. Thoma, Z. Phys. C **66**, 491 (1995).
[34] Y. Hidaka, D. Satow, and T. Kunihiro, arXiv:1105.0423; Nucl. Phys. **A876**, 93 (2012).
[35] J.-P. Blaizot and D. Satow, Phys. Rev. D **89**, 096001 (2014).
[36] J. S. Schwinger, J. Math. Phys. (N.Y.) **2**, 407 (1961); L. V. Keldysh, Zh. Eksp. Teor. Fiz. **47**, 1515 (1964) [Sov. Phys. JETP **20**, 1018 (1965)].
[37] A. Das, *Finite temperature field theory* (World Scientific, Singapore, 1997).
[38] R. L. Kobes and G. W. Semenoff, Nucl. Phys. **B260**, 714 (1985); **B272**, 329 (1986).
[39] S. Sarkar, Adv. High Energy Phys. **2013**, 627137 (2013).
[40] S. Ghosh, Int. J. Mod. Phys. A **29**, 1450054 (2014).